



TECHNISCHE
UNIVERSITÄT
WIEN

Vienna University of Technology

DIPLOMARBEIT

Advanced tight-binding descriptions of graphene

ausgeführt am

Institut für Theoretische Physik
der Technischen Universität Wien

unter der Anleitung von

Univ.Prof. Dr. Joachim Burgdörfer
Univ.Ass. Dr. Florian Libisch

durch

Rafael Reiter BSc

Marktgasse 4/1/2
1090 Wien

Wien, 21. Juli 2014

Unterschrift

Quantitatively accurate tight-binding parameters can be created from DFT band structures using Maximally Localized Wannier Functions, faster and for more complex materials than with fitting procedures. We propose a tight-binding parameter building block system for graphene that encapsulates defects like edges and missing atoms for reuse in bigger structures. We illustrate the concept for graphene nanoribbons. Towards a tight-binding description of the graphene-Ni interface, we show that Wannier orbitals can accurately reproduce the complicated band structure of a graphene-Ni slab.

Additionally, we explore methods to extract tight-binding parameters from high-level quantum chemistry calculations and calculate Hartree-Fock expectation values of natural orbitals of acenes.

Contents

1. Introduction	7
2. Fundamentals	9
2.1. Ab-initio methods	9
2.1.1. Density functional theory	9
2.1.2. Quantum chemistry methods	9
2.2. Tight-binding formalism	10
2.3. Nearest-neighbor approximation	12
2.3.1. Slater-Koster parameterization	14
2.4. Constructing a tight-binding Hamiltonian for a band structure	14
2.5. Graphene	17
2.5.1. Band structure	20
2.5.2. Graphene nanoribbons	21
2.6. Wannier orbitals	21
2.6.1. Maximally Localized Wannier Functions (MLWF)	22
2.6.2. Tight-binding fit vs. Wannier orbitals	24
2.6.3. Choice of energy, k-points and guess orbitals	24
2.6.4. Tight-binding parameters	25
2.6.5. Real-space representation	26
2.6.6. Accuracy of band selection and band reproduction	26
2.7. Building block system for tight-binding parameters	26
3. Infinite graphene sheets	28
3.1. Nearest-neighbor parameterization	28
3.1.1. Fitting procedure to DFT band structures	28
3.1.2. 1 st -nearest-neighbor parameterization	29
3.1.3. 3 rd -nearest-neighbor parameterization and higher	30
3.1.4. Computational effort	31
3.2. Parameterization using MLWFs	31
3.3. Conclusions	34
4. Defect structures	38
4.1. Zigzag graphene nanoribbons	39
4.1.1. DFT calculation	39
4.1.2. Wannier orbitals for a nanoribbon	41
4.1.3. Band structure from graphene Wannier parameters	45
4.1.4. Application of building blocks	47

4.2. Conclusions	49
5. Graphene on Ni(111)	51
5.1. Model system	51
5.2. Face-centered cubic (fcc) crystal lattice	51
5.3. Wannier orbitals of face-centered cubic Nickel	52
5.4. Wannier orbitals of graphene on Ni(111)	54
5.5. Conclusions	54
6. Polycyclic aromatic hydrocarbons	59
6.1. Comparison of quantum chemistry methods and tight-binding	60
6.2. Disentangling fractionally occupied natural orbitals	65
6.3. Hartree-Fock expectation values	66
6.4. Conclusions	67
A. Appendix	68
A.1. Software	68

1. Introduction

Graphene, a carbon-based, two-dimensional solid [25, 24, 26], features unique electrical and mechanical properties, mainly due to its peculiar linear band structure at energies near the Fermi level [32, 23]. The material gives rise to many new and intriguing applications including high-precision mechanical or chemical sensors, ultrafast single-electron transistors [37] or spintronic devices.

The electronic properties of infinite graphene are theoretically well understood. However, the description of dots, ribbons and finite-sized structures in general, as well as realistic materials which are subject to impurities, is still a challenging task in theoretical physics.

Finite-sized structures play an especially important role. Due to the gapless band structure of graphene, confinement using electrostatic potentials is not possible. Devices are manufactured by cutting or etching, resulting in rough edges that influence transport properties.

Graphene quantum dots [22, 7, 38, 16, 8, 15] experience Coulomb blockade and quantum confinement effects; graphene nanoribbons [31, 14] are also of increasing interest due to their promise of a band gap [35], overcoming the gapless band structure of truly two-dimensional graphene. In particular, their overall semiconducting behavior allows the fabrication of graphene field-effect transistors, tunnelling barriers and quantum devices.

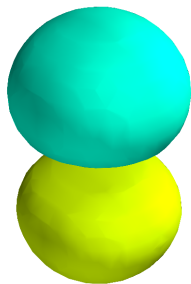
The quantum mechanical description of dots, ribbons and other devices with edges and impurities requires a method that can handle up to millions of atoms, but still describes the physics introduced by defects.

Of all quantum mechanical descriptions of the electronic properties of crystals, tight-binding is one of the simplest and crudest, but also one of the fastest – and the current method of choice for systems with millions of atoms. However, tight-binding needs input from other electronic structure calculations. There are several ways how to generate this input and translate it to tight-binding parameters. We investigate the application of Maximally Localized Wannier Functions (MLWFs) replacing the commonly used band structure fitting procedure. The MLWF procedure is a promising candidate to improve accuracy and versatility of tight-binding. In conjunction with density-functional theory (DFT) software, we use it to streamline the workflow for creating tight-binding parameters from DFT input. Real-space orbital representations of the basis orbitals are available, and much bigger unit cells can be handled than with the usual fitting procedure. It is possible to process DFT calculations of whole nanoribbons, defective supercells or surfaces.

The logical next step after the creation of tight-binding parameters for supercells is a building block system: We derive parameters from a bulk crystal calculation and join them with parameters that we derive from a defective supercell calculation. This

improves the accuracy for various systems with arbitrary size using a finite set of building blocks that describe the individual defects that occur in the system.

The description of defective systems with millions of atoms is of high relevance in experimental physics. First nearest neighbor tight-binding is still very popular in the field because of its simplicity. With a simple workflow of standard DFT and MLWF software, we aim to bring high-precision tight-binding to the experimental physics community.



2. Fundamentals

2.1. Ab-initio methods

2.1.1. Density functional theory

Density functional theory [27] is a method to calculate the energy of the electronic ground state of a system. The energy is expressed as a functional of the electronic density. This reduces the dimensionality of the problem from $3N$ (N is the number of electrons) to 3, making the description of many-electron systems possible. The commonly used *local density approximation* (LDA) refers to the approximation method for the exchange and correlation energy which is, in case of the LDA, approximated with the exchange-correlation energy of a free electron gas.

DFT can be used to calculate

- the total energy: by finding atomic positions that minimize the total electronic energy, material structures can be predicted.
- the band structure: many DFT codes use a plane wave basis set, which makes it easy to impose Bloch boundary conditions and calculate the energies of an electron with a certain Bloch wave vector k . Since DFT is, in principle, a method that calculates the ground state energy of a system, the energies of a single electron (called Kohn-Sham energies – as depicted in the band structure) are not physically meaningful, but are still used as an approximation for the single-particle energies.

2.1.2. Quantum chemistry methods

Quantum chemistry methods are electronic structure algorithms that are based on the *Hartree-Fock* method and describe the many-particle wave function as a single Slater determinant (Hartree-Fock) or a linear combination of those (post Hartree-Fock) [9]. The computational cost depends on the method, but is high in all cases (compared to other methods). Quantum chemistry methods are used to calculate the electronic structure of molecules. Usually, a localized basis is used, so that the calculation of band structures is not possible because the Bloch boundary conditions cannot be fulfilled.

Like in DFT, single-electron energies may be assigned to electronic orbitals, but are not always meaningful (the total energy is the important value). In Hartree-Fock, they can be interpreted as the ionization energies (see [9], p. 64). In other quantum chemistry methods, the single-particle energies have no obvious analogon.

2.2. Tight-binding formalism

Tight-binding is a simple approach for electronic structure calculations, but also the method of choice for large systems. In chemistry, the approach is called *linear combination of atomic orbitals* (LCAO). The idea is the following: Since we are interested in chemical or transport properties, we assume that only the valence electrons of the single atoms (the electrons of the outer shell) play a role because the other electrons remain localized at the core. We further assume that the wavefunction of a molecule or a bulk material can be described by adding up the atomic wavefunctions (which are well-localized around each atom) plus a small correction. In mathematical terms, this is a linear combination of the occupied atomic orbitals plus some unoccupied atomic orbitals for correction:

$$|\psi\rangle = \sum_n a_n |\phi_n\rangle, \quad (2.1)$$

where $|\psi\rangle$ is a molecular single-electron wavefunction, n runs over all basis orbitals on all sites (meaning atoms), a_n are the coefficients and $|\phi_n\rangle$ are the basis orbitals. The coefficients a_n can be understood as expansion coefficients in terms of the basis orbitals. In a particular state, some a_n may be much larger than others and therefore dominate the characteristics of the eigenstate.

Usually, the basis consists of the valence states that are occupied in the free atom; e.g. in carbon, the valence electrons are two electrons in 2s and four electrons in $2p_x$, $2p_y$ and $2p_z$. Of course, even in the free atom case, the many-body electronic wavefunction does not exactly consist of those orbitals (because of the electron-electron interaction). They are only valid for the hydrogen problem. Still, it is a good basis to start out with.

The demands on the tight-binding calculation influences the choice of orbitals. For example, if one is only interested in low-energy transportation properties of graphene, one can use only the p_z orbitals, which reduces the calculation effort significantly.

The single-electron Schrödinger equation can be solved in terms of a linear algebra problem by inserting Eq. (2.1) into the Schrödinger equation $H|\psi\rangle = E|\psi\rangle$ and applying $\langle\phi_m|$ from the left:

$$\sum_n \langle\phi_m| H |\phi_n\rangle a_n = E \sum_n \langle\phi_m|\phi_n\rangle a_n$$

Since $H_{mn} = \langle\phi_m| H |\phi_n\rangle$ and $S_{mn} = \langle\phi_m|\phi_n\rangle$ are $m \times n$ matrices and a_n is a vector, this is a generalized eigenvalue problem of the form $Ha = E Sa$. If the orbitals are orthogonal to each other and S is therefore diagonal ($S_{mn} = \delta_{mn}$), it reduces to an ordinary eigenvalue problem.

$$\sum_n H_{mn} a_n = E a_m \quad (2.2)$$

After solving for E and a_n , we can insert the a_n into Eq. (2.1) to retrieve the wave function in real space. The size of the Hamiltonian is determined by the number of

orbitals. For n_{atom} atoms and n_{orb} orbitals per atom, there are $n_{atom}n_{orb}$ orbitals in total.

Since the basis is not complete (we select the basis functions $|\phi_n\rangle$ by an educated guess), we cannot describe every $|\psi\rangle$ with our restricted basis and equation (2.1) is only approximately valid.

The crucial element is, of course, the matrix H_{mn} and its entries $\langle\phi_m|H|\phi_n\rangle$. The many-particle electronic Hamiltonian in Born-Oppenheimer approximation (meaning that the ions have a large mass compared to the electrons, and their movement can be decoupled) is

$$H = \sum_n \frac{p_n^2}{2m_e} + \frac{1}{4\pi\epsilon_0} \left(\frac{1}{2} \sum_{n,n'} \frac{e^2}{|r_n - r_{n'}|} + \sum_{n,m} \frac{Ne}{|r_n - R_m|} \right) \quad (2.3)$$

This is a many-particle Hamiltonian, while tight-binding is a one-electron approximation. Thus, tight-binding takes a similar approach as density functional theory [27] and Hartree-Fock theory [9] and assumes that the electron-electron interaction can be described by considering non-interacting (meaning: not with other electrons) particles in a potential that contains the influence of all other electrons. In contrast to the other methods, this effective potential V_{eff} is assumed to be independent of the solution, and therefore no self-consistency is imposed. For additional informations on this approximation, see [13, pp. 5-8].

The tight-binding Hamiltonian and its matrix elements are given by

$$H^{TB} = \sum_n \frac{p_n^2}{2m_e} + V_{\text{eff}} \quad H_{mn}^{TB} = \langle\varphi_m| \sum_n \frac{p_n^2}{2m_e} + V_{\text{eff}} |\varphi_n\rangle$$

At this point, the expression for V_{eff} is not known, and the matrix elements can not be evaluated. This is why tight-binding is not an ab-initio method: the matrix elements H_{mn} are determined by comparing the results of the tight-binding calculation (eigenvalues, eigenvectors and other properties calculated from them) to other methods like DFT and Hartree-Fock. *The matrix elements are fit to reproduce existing data.* The assumption is that those matrix elements can later be used for (slightly) different or bigger systems. The most common approach is to use matrix elements obtained from a fit to a DFT band structure (which describes the bulk properties of an extended material) for a finite-sized system (ribbon, large molecule etc.).

In the following, we distinguish between the diagonal (called on-site parameters/elements, denoted by ε) and the off-diagonal (called hopping parameters/elements, denoted by γ or γ) matrix elements H_{mn} , for example:

$$\begin{aligned} \varepsilon_i = H_{ii} &= \langle\varphi_i| H^{TB} |\varphi_i\rangle \\ \gamma_{ij} = H_{ij} &= \langle\varphi_i| H^{TB} |\varphi_j\rangle \end{aligned}$$

The nomenclature comes from the time evolution: if we assume that the electron is in a state $|\varphi_i\rangle$, the on-site and hopping matrix entries determine the probability that

the electron will stay in $|\varphi_i\rangle$ or “hop” into an other orbital $|\varphi_i\rangle$, respectively, in a time evolution $\exp(-i\mathbf{H}t)|\varphi_i\rangle$.

The number of parameters that can/have to be adjusted to match data from other sources is smaller than the number of matrix elements $(n_{atom}n_{orb})^2 = n_{total}^2$ because of the Hermiticity of the matrix. If all basis orbitals are real, the matrix is symmetric, and the number of parameters is $\frac{1}{2}n_{total}(n_{total} + 1)$. This number can be reduced further:

- The on-site parameters of spherical-harmonic orbitals of equal type (s,p,d,...) on the same atom have equal on-site parameters ($\varepsilon_s, \varepsilon_p$ etc.) because of translational symmetry.
- On-site as well as hopping parameters are equal if atoms (or pairs of atoms) are equal due to the symmetry of the system.
- The hopping parameters γ_{ij} between spherical-harmonic orbitals on the same atom are zero, as in the free-atom case.
- The matrix elements H_{mn} between orbitals are becoming smaller with growing distance. If the distance exceeds a certain radius, the hopping elements are set to 0. Usually, the hopping elements between an atom and its first n neighbours are taken into account (see section 2.3).
- Using the Slater-Koster (SK) parameterization, the matrix elements can be parameterized using symmetry so that the hopping matrix elements between a pair of atoms can be described by a smaller number of parameters. For example, the 16 hopping matrix elements (counting the matrix elements of all orbitals of one atom with all orbitals of the other atom, because on-site parameters are not affected by the SK-parameterization and intraatomic hopping is set to 0; additionally, $H_{ij} = H_{ji}$, so finally number of atom pairs \times number of orbitals per atom²) between two atoms that both have 1 s-type and 3 p-type orbitals (16 nonzero hopping elements) can be reduced to 4 parameters (see section 2.3.1).

It is important to realize that, due to the fitting process used to obtain the tight-binding Hamiltonian H_{TB} , we don’t actually need to know what the basis orbitals look like in real space. If we use Slater-Koster parameterization, we implicitly use orbitals that have the same spherical symmetric properties as the spherical harmonics. Since they were situated around the nucleus in the free-atom case, it is probable that they still do so.

2.3. Nearest-neighbor approximation

The nearest neighbour approximation makes use of the fact that the Hamiltonian matrix elements H_{mn} between basis orbitals $|\phi_m\rangle$ and $|\phi_n\rangle$ become smaller as their distance increases. Hopping matrix elements between orbitals whose distance is greater than a certain threshold are set to zero. In a bulk material, there are always groups of atoms which have the same distance to a given atom (due to the symmetries of the

material). After numbering those groups according to the distance, we can introduce nearest-neighbour, second-nearest-neighbour approximations etc.

For a given carbon atom in graphene, all atoms that have the same distance to the first atom also have the same matrix element H_{mn} . They belong to the same nearest-neighbor group (same color in Fig. 2.1). Using one s-type and three p-type orbitals, there are 4 Slater-Koster parameters per pair of atoms. Because of the symmetry, the same 4 parameters can be used for the Hamiltonian matrix elements between any atom and its neighbor with the same distance. This means that the number of parameters for bulk graphene is $4N + 2$, where N is the number of considered nearest-neighbor groups.

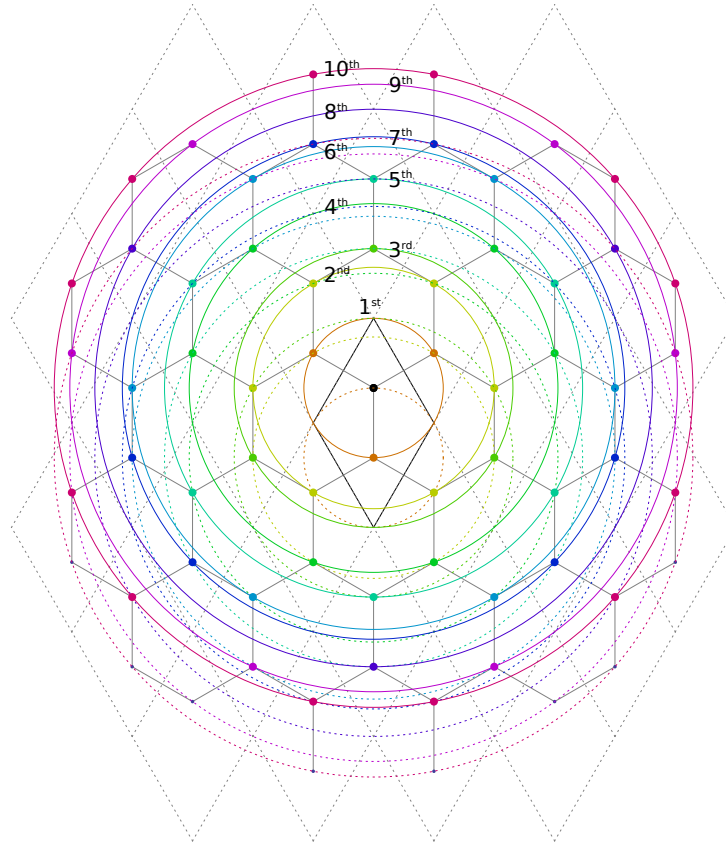


Figure 2.1.: Neighbor classification in graphene. The unit cell marked by the black rhombus is the main cell; the grey dotted rhombuses mark the neighbor cells. Each solid circle classifies the n^{th} nearest neighbor group of the upper (black) carbon atom of the main cell. The dotted circles do the same for the lower atom of the main cell. Up to the 10^{th} nearest neighbors (outermost ring), the atoms are contained within 34 basis cells around the main cell (64 atoms).

$$\begin{aligned}
\langle s | H | s \rangle &= V_{ss\sigma} \\
\langle s | H | p_{x/y/z} \rangle &= l V_{sp\sigma} \\
\langle p_x | H | p_x \rangle &= l^2 V_{pp\sigma} + (1 - l^2) V_{pp\pi} \\
\langle p_x | H | p_y \rangle &= lm(V_{pp\sigma} - V_{pp\pi}) \\
\langle p_x | H | p_z \rangle &= ln(V_{pp\sigma} - V_{pp\pi})
\end{aligned}$$

Table 2.1.: Part of the Slater and Koster table [34] of interatomic matrix elements for s-type and p-type orbitals. The bra and ket orbitals are located on different atoms. l , m and n are the x , y and z components of the unit vector pointing from the bra to the ket orbital. More parameterizations exist for d-, f- and g-orbitals.

2.3.1. Slater-Koster parameterization

Slater and Koster showed that the hopping matrix elements between basis orbitals with spherical harmonics characteristics can be greatly simplified (see [34], [6, pp. 194-197] and [39, pp. 120-124]). For a given pair of atoms, the hopping matrix elements between two p-type orbitals depends on two parameters, regardless of their orientation; the matrix elements between an s-type and a p-type orbital depend on one parameter etc. For an orbital basis with s-type and p-type orbitals, there are four parameters: $V_{ss\sigma}$, $V_{sp\sigma}$, $V_{pp\sigma}$ and $V_{pp\pi}$. The actual matrix elements are derived from those parameters according to table 2.1.

The parameters l , m and n (see Table 2.1) are the x , y and z component of the unit vector that points from atom i (corresponding to the bra orbital of the Hamiltonian matrix element) to atom j (corresponding to the ket orbital of the Hamiltonian matrix element):

$$\begin{pmatrix} l \\ m \\ n \end{pmatrix} = \frac{\vec{r}_{ij}}{|\vec{r}_{ij}|}$$

We vary the Slater-Koster parameters so that the results of the tight-binding calculation fit ab-initio data.

In the case of 1 s-type and 3 p-type orbitals, the Slater-Koster parameterization reduces the number of necessary parameters from 7 to 4.

2.4. Constructing a tight-binding Hamiltonian for a band structure

The band structure of a material is a way to describe the electronic properties of a crystal that consists of an infinite number of copies of a unit cell which are arranged in a lattice

[11]. At each lattice point $\vec{R}_{lmn} = l\vec{a}_1 + m\vec{a}_2 + n\vec{a}_3$ (l, m, n are integers, and \vec{a}_i are the lattice basis vectors – all \vec{R}_{lmn} are called lattice vectors), there is a copy of the unit cell. This means that the crystal has a discrete translational symmetry. The Hamiltonian of the Schrödinger equation has the same symmetries, and according to the Bloch theorem [2], every eigenstate fulfills the requirement

$$\psi_{\vec{k}}(\vec{r} + \vec{R}) = e^{i\vec{k}\vec{R}}\psi_{\vec{k}}(\vec{r}) \quad (2.4)$$

\vec{R} is any lattice vector, and \vec{k} is a reciprocal lattice vector within the first Brillouin zone and, at the same time, a quantum number for the eigenstate.

The band structure is a plot of the eigenvalues of the Schrödinger equation as a function of the Bloch wave number \vec{k} . This means that we need a way to calculate all solutions for a given \vec{k} .

For the calculation, only the solutions in one unit cell are necessary because the solution anywhere else can be calculated from the first cell using Eq. 2.4.

If we want to solve the Schrödinger equation as a partial differential equation (without an orbital basis, e.g. with a discretization scheme), boundary conditions have to be supplied, and this is where the Bloch theorem enters. Because of Eq. 2.4, the wave function $\psi(\vec{r})$ at a point \vec{r} at the unit cell boundary has to be equal to the wave function $\psi(\vec{r} - \vec{R})$ at the boundary point $\vec{r} - \vec{R}$ multiplied with a phase factor $e^{i\vec{k}\vec{R}}$. The same holds for the derivative at the boundary, and thus, all necessary boundary conditions are supplied.

If an orbital basis is used to solve the equation, the implementation of the Bloch theorem is quite different. As an example, we will look at a unit cell in a one-dimensional system with one atom and two orbitals on it (Fig. 2.2).

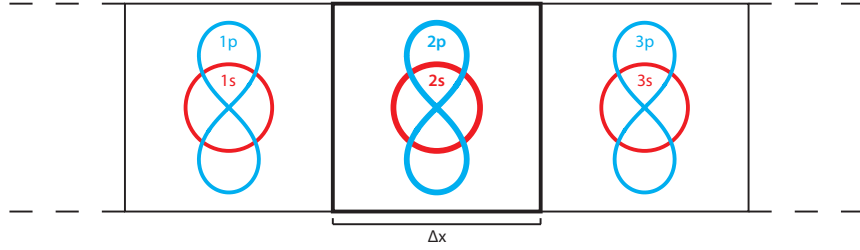


Figure 2.2.: Example unit cell with one atom and two orbitals (s-type and p_z -type).

The Schrödinger equation “in this part” of the (infinite) system with nearest-neighbour approximation looks like this:

$$\begin{pmatrix} \dots & \dots & \dots & \dots & \dots & \dots & \dots & \dots \\ \dots & \varepsilon_s & 0 & V_{ss\sigma} & V_{sp\sigma} & 0 & 0 & \dots \\ \dots & 0 & \varepsilon_p & V_{sp\sigma} & V_{pp\pi} & 0 & 0 & \dots \\ \dots & V_{ss\sigma} & V_{sp\sigma} & \varepsilon_s & 0 & V_{ss\sigma} & V_{sp\sigma} & \dots \\ \dots & V_{sp\sigma} & V_{pp\pi} & 0 & \varepsilon_p & V_{sp\sigma} & V_{pp\pi} & \dots \\ \dots & 0 & 0 & V_{ss\sigma} & V_{sp\sigma} & \varepsilon_s & 0 & \dots \\ \dots & 0 & 0 & V_{sp\sigma} & V_{pp\pi} & 0 & \varepsilon_p & \dots \\ \dots & \dots & \dots & \dots & \dots & \dots & \dots & \dots \end{pmatrix} \begin{pmatrix} \dots \\ a_{1s} \\ a_{1p} \\ a_{2s} \\ a_{2p} \\ a_{3s} \\ a_{3p} \\ \dots \end{pmatrix} = E \begin{pmatrix} \dots \\ a_{1s} \\ a_{1p} \\ a_{2s} \\ a_{2p} \\ a_{3s} \\ a_{3p} \\ \dots \end{pmatrix} \quad (2.5)$$

According to the Bloch theorem (Eq. 2.4) the solutions in the unit cells have to be related by a phase factor, and therefore, also the coefficients have to be, according to their positions:

$$\begin{aligned} a_{1s} &= e^{-ik\Delta x} a_{2s} \\ a_{3s} &= e^{ik\Delta x} a_{2s} \end{aligned}$$

The same identities are valid for the p-type orbitals, and for any orbital in the infinite crystal – with the according phase factor. They can be inserted into the vectors of the Schrödinger equation (Eq. 2.5):

$$\begin{pmatrix} \dots \\ a_{1s} \\ a_{1p} \\ a_{2s} \\ a_{2p} \\ a_{3s} \\ a_{3p} \\ \dots \end{pmatrix} = \begin{pmatrix} \dots \\ e^{-ik\Delta x} a_{2s} \\ e^{-ik\Delta x} a_{2p} \\ a_{2s} \\ a_{2p} \\ e^{ik\Delta x} a_{2s} \\ e^{ik\Delta x} a_{2p} \\ \dots \end{pmatrix}$$

The former six coefficients were reduced to two: a_{2s} and a_{2p} . Any other coefficient in the crystal can also be replaced by $e^{i\vec{k}\vec{R}}$ with the corresponding lattice vector \vec{R} . This can be used to simplify the matrix equation. To illustrate this, let's look at the a_{2s} equation (third line, excluding the “dot” line) of the above eigenvalue problem:

$$\dots + V_{ss\sigma} a_{1s} + V_{sp\sigma} a_{1p} + \varepsilon_s a_{2s} + 0 a_{2p} + V_{ss\sigma} a_{3s} + V_{sp\sigma} a_{3p} + \dots = E a_{2s}$$

After inserting the identities and reordering, the equation reads:

$$\begin{aligned} \dots + V_{ss\sigma} e^{-ik\Delta x} a_{2s} + V_{sp\sigma} e^{-ik\Delta x} a_{2p} + \varepsilon_s a_{2s} + 0 a_{2p} + V_{ss\sigma} e^{ik\Delta x} a_{2s} + V_{sp\sigma} e^{ik\Delta x} a_{2p} + \dots &= E a_{2s} \\ (\dots + V_{ss\sigma} e^{-ik\Delta x} + \varepsilon_s + V_{ss\sigma} e^{ik\Delta x} + \dots) a_{2s} + (\dots + V_{sp\sigma} e^{-ik\Delta x} + V_{sp\sigma} e^{ik\Delta x} + \dots) a_{2p} &= E a_{2s} \end{aligned}$$

This can again be written as a matrix, but the dimension was reduced from ∞ to 2, and the matrix elements were truncated as described by the equations above. If the same

algorithm is applied to all equations of the eigenvalue problem, every second equation becomes identical, so that all equations but two can be dropped:

$$\begin{pmatrix} \dots + V_{ss\sigma}e^{-ik\Delta x} + \varepsilon_s + V_{ss\sigma}e^{ik\Delta x} + \dots & \dots + V_{sp\sigma}e^{-ik\Delta x} + V_{sp\sigma}e^{ik\Delta x} + \dots \\ \dots + V_{sp\sigma}e^{-ik\Delta x} + V_{sp\sigma}e^{ik\Delta x} + \dots & \dots + V_{pp\pi}e^{-ik\Delta x} + \varepsilon_p + V_{pp\pi}e^{ik\Delta x} + \dots \end{pmatrix} \begin{pmatrix} a_{2s} \\ a_{2p} \end{pmatrix} = E \begin{pmatrix} a_{2s} \\ a_{2p} \end{pmatrix}$$

If a nearest-neighbour approximation is used, the hopping parameters between remote unit cells are set to zero. In this example, we use a nearest-neighbour approximation, so all the “dot” parts are zero, and the equation reads:

$$\begin{pmatrix} V_{ss\sigma}e^{-ik\Delta x} + \varepsilon_s + V_{ss\sigma}e^{ik\Delta x} & V_{sp\sigma}e^{-ik\Delta x} + V_{sp\sigma}e^{ik\Delta x} \\ V_{sp\sigma}e^{-ik\Delta x} + V_{sp\sigma}e^{ik\Delta x} & V_{pp\pi}e^{-ik\Delta x} + \varepsilon_p + V_{pp\pi}e^{ik\Delta x} \end{pmatrix} \begin{pmatrix} a_{2s} \\ a_{2p} \end{pmatrix} = E \begin{pmatrix} a_{2s} \\ a_{2p} \end{pmatrix}$$

From this example, we can deduct an “effective” algorithm:

- Set up the Hamiltonian for a system consisting of a “central” unit cell and all other unit cells you want to include for an n-th-nearest neighbour-approximation (e.g. 8 adjacent unit cells for a 3rd-NN-approximation in graphene – see section 2.3)
- Take the rows corresponding to the orbitals in the central unit cell. Multiply each column n with the Bloch phase factor (it depends on \vec{k} !) that corresponds to the position of the orbital φ_n . The central unit cell can have the Bloch phase factor 1 (that would be the obvious way to do it), but this is not necessary.
- Add up the columns that correspond to the same orbital in different unit cells. The resulting square matrix is your band structure Hamiltonian $H(\vec{k})$.

The dimension of the eigenvalue problem is given by the number of orbitals in a unit cell; in the case of graphene (2 atoms per unit cell) and s, p_x , p_y and p_z as basis orbitals, there are 8 orbitals.

2.5. Graphene

Graphene is a (theoretically) infinitely large, two-dimensional crystal. We will derive the lattice vectors and atom positions, starting with the the lattice constant $a = 2.461 \text{ \AA}$ from [29]) using figure 2.3.

Graphene consists of a hexagon lattice of carbon atoms. The lattice vectors are of equal length and form an angle of 60 degrees (or 120 degrees). The carbon atoms are situated on the hexagon corners. The lattice vectors a_1 and a_2 connect the centers of the hexagons. They also form a unit cell (dashed lines and thick line) containing two carbon atoms, labeled atom A and atom B (they form two trigonal sublattices labeled A and B).

The lattice constant a is the distance between two atoms in adjacent unit cells which both belong to the same sublattice (A or B). The distance c between two adjacent carbon

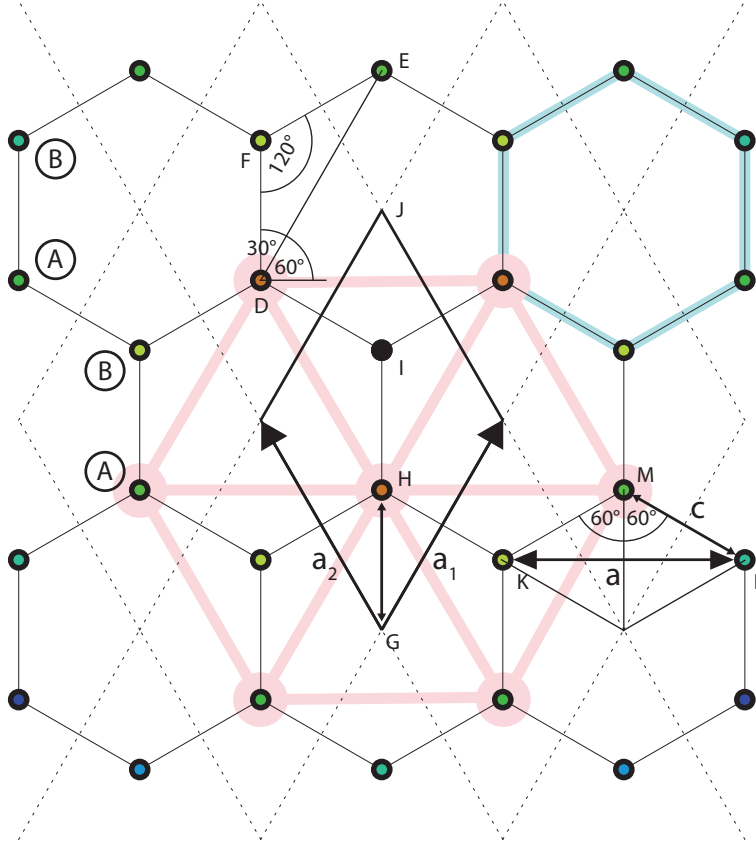


Figure 2.3.: Schematic illustration of the graphene geometry. The black rhombus is the reference cell, the dashed lines mark neighboring cells. a_1 and a_2 are the lattice vectors. The blue hexagon and the similar black hexagons show another possible grid of unit cells (the Wigner-Seitz unit cell – in contrast to the dashed rhombuses). A and B label the sublattices.

atoms (e.g. LM) can be calculated using the triangle KLM . Because a hexagon consists of six equilateral triangles which have 60 degree angles, the angle $\angle LMK$ is 120 degrees and $LM = \frac{\frac{KL}{2}}{\sin 60^\circ} = \frac{a}{2 \sin 60^\circ} = \frac{a}{\sqrt{3}} = c$.

The lattice vectors a_1 and a_2 are calculated using the triangle DEF . Because the angle $\angle DFE$ is 120 degrees (see above), the other angles of this triangle are 30° , and therefore the angle between a horizontal line and the vector DE is 60 degrees. The distance $|DE|$ is a , and so the vector DE , which is equivalent to a_1 , can be found by rotating a horizontal vector with the length a by 60 degrees:

$$a_1 = DE = \begin{pmatrix} \cos 60^\circ & -\sin 60^\circ \\ \sin 60^\circ & \cos 60^\circ \end{pmatrix} \begin{pmatrix} a \\ 0 \end{pmatrix} = \frac{a}{2} \begin{pmatrix} 1 \\ \sqrt{3} \end{pmatrix}.$$

a_2 is the mirror image of a_1 with respect to the vertical axis, so we just have to flip

the sign of the x-component:

$$a_2 = \frac{a}{2} \begin{pmatrix} -1 \\ \sqrt{3} \end{pmatrix}.$$

Because a hexagon consists of six equilateral triangles, the distance between the center and a corner (e.g. GH) is also $c = \frac{a}{\sqrt{3}}$. Thus, GH , HI and IJ are all of equal length, and the positions of the carbon atoms (within a unit cell) are

$$b_1 = GH = \frac{1}{3}GJ = \frac{1}{3}(a_1 + a_2) = \begin{pmatrix} 0 \\ c \end{pmatrix} = \frac{1}{\sqrt{3}} \begin{pmatrix} 0 \\ a \end{pmatrix}$$

$$b_2 = GI = \frac{2}{3}GJ = \frac{2}{3}(a_1 + a_2) = \begin{pmatrix} 0 \\ 2c \end{pmatrix} = \frac{2}{\sqrt{3}} \begin{pmatrix} 0 \\ a \end{pmatrix}$$

The hexagonal lattice is named after the symmetric unit cell (light blue line) which is the Wigner-Seitz cell and an equal alternative (with the same lattice vectors) to the rhombic unit cell (thick black line). Additionally, each sublattice (A or B) form a hexagon-like structure (pink lines) which has an additional atom in the center of the hexagon.

The reciprocal unit cell (see Fig. 2.4) is also hexagonal, but rotated by 90° with respect to the unit cell in real space. Because of symmetry, $1/12$ of the reciprocal unit cell already contains the entire band structure. Since the plot $E(k_x, k_y)$ is very hard to represent in 2D (because there are several values of E for each k point), one plots the values of E along the path encircling the relevant $1/12$ of the band structure.

The reciprocal lattice vectors are usually found using the cross product, so that $a_i \cdot c_j = 2\pi n \delta_{ij}$ is fulfilled. In two dimensions, this can be accomplished by rotating the lattice vectors by 90 degrees clockwise:

$$c_1 = \frac{2\pi}{\det(a_1 a_2)} \begin{pmatrix} 0 & 1 \\ -1 & 0 \end{pmatrix} a_2 = \frac{2\pi}{\frac{1}{2}\sqrt{3}a^2} \frac{a}{2} \begin{pmatrix} \sqrt{3} \\ 1 \end{pmatrix} = \frac{2\pi}{a} \begin{pmatrix} 1 \\ \frac{1}{\sqrt{3}} \end{pmatrix}$$

$$c_2 = \frac{2\pi}{\det(a_1 a_2)} \begin{pmatrix} 0 & 1 \\ -1 & 0 \end{pmatrix} a_1 = \frac{2\pi}{a} \begin{pmatrix} -1 \\ \frac{1}{\sqrt{3}} \end{pmatrix}.$$

$\det(a_1 a_2)$ is the determinant of the matrix consisting of a_1 and a_2 and ensures that $a_i c_i = 2\pi n$ (easily proven by inserting the vector components).

The reciprocal vectors can be generated equivalently using a unit vector in z direction as a third lattice vector.

The special points in k -space in terms of the reciprocal lattice vectors are: $\Gamma = (0, 0)$, $K = \frac{1}{3}(c_1 - c_2)$ and $M = \frac{1}{2}c_1$. Because of the periodicity of the band structure, some corners of the unit cell are equivalent, e.g. K is also the lower left corner of the hexagon.

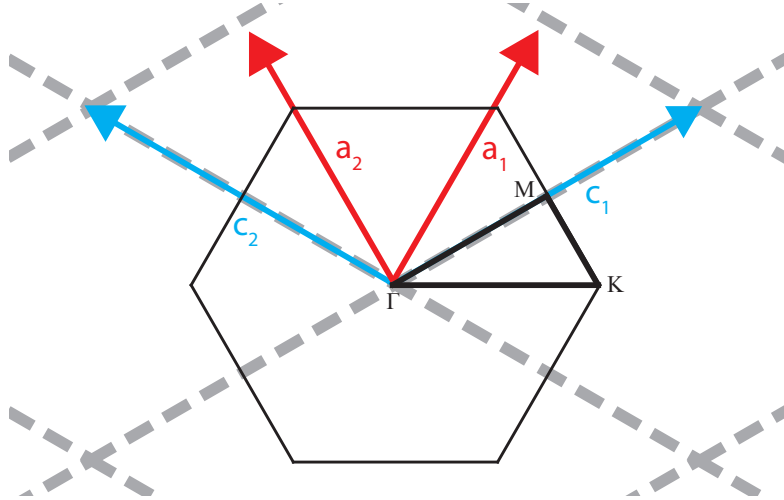


Figure 2.4.: Reciprocal lattice of graphene (given by the reciprocal lattice vectors c_1 and c_2 , blue), unit cell (dashed grey) and the usual band structure plot path $\Gamma K M \Gamma$. a_1 and a_2 are the lattice vectors. The black hexagon is the Wigner-Seitz cell.

2.5.1. Band structure

The graphene band structure consists of three main parts:

- The σ system: lower three bands. They can be described by sp^2 -like hybrid orbitals which are responsible for the chemical bonding of the carbon atoms and have most electron density on the connections between the carbon atoms. They are energetically well below E_F and do not participate in electron conductance; for the same reason, the chemical bonding is strong. They are completely occupied.
- The π system: fourth and fifth band. They can be described by p_z -like states. The lower band (called π band) is occupied, the upper band (π^* band) is not. Conductance happens when electrons are excited from the π to the π^* band.
- Bands far above E_F , mainly bands with no atomic orbital characteristics.

The phrasing "can be described by" refers to the fact that the Bloch states in those bands exclusively consist of the mentioned basis set. "like" means that those basis orbitals look very much, but not exactly like the spherical harmonics which give them their name.

The graphene band structure $E(k_x, k_y)$ is usually plotted along a path in the reciprocal space, namely the triangle made up of the points Γ , K and M (see Fig. 2.4).

It's interesting to compare the graphene band structure to the dispersion relation of a free electron (pure Laplace equation) with zone folding (Fig. 2.5). Although the electrons are massively influenced by the atomic cores, they still look very much like the free electron bands (which explains the success of the Sommerfeld theory).

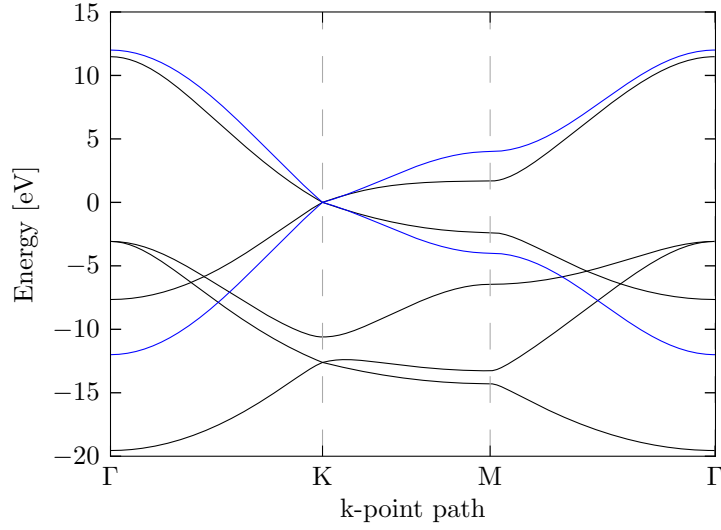


Figure 2.5.: Graphene DFT band structure (black) and the dispersion relations of two free electrons (blue), one with positive, one with negative mass (scaled to resemble the other bands in magnitude). The qualitative shape of the latter and the graphene π system is similar.

2.5.2. Graphene nanoribbons

A graphene nanoribbon can be described by "cutting out" a stripe from an infinite graphene sheet. There are two different ways to do that, which differ in the edge configuration: zigzag (zzGNR) and armchair (aGNR – see Fig. 2.7). Fig. 2.6 shows the band structures.

Zigzag ribbons show an interesting property, the so-called *edge states*. The states in the flat bands around E_F (which contribute to conductance) are exclusively located at the edges. This property easily becomes distorted as soon as the zigzag edge has a defect.

2.6. Wannier orbitals

Wannier orbitals $w_{n\mathbf{R}}(\mathbf{r})$ [5, 12, 33, 36, 20, 19] are localized orbitals which are obtained from Bloch states using a unitary transformation. Usually, those Bloch states are the Kohn-Sham orbitals $\psi_{m\mathbf{k}}(\mathbf{r})$ from a DFT calculation. Wannier orbitals are defined as

$$w_{n\mathbf{R}}(\mathbf{r}) = \frac{V}{(2\pi)^3} \int_{BZ} \left[\sum_m U_{mn}^{(\mathbf{k})} \psi_{m\mathbf{k}}(\mathbf{r}) \right] e^{-i\mathbf{k} \cdot \mathbf{R}} d\mathbf{k}$$

The resulting orbital $w_{n\mathbf{R}}(\mathbf{r})$ is localized centered on the lattice site \mathbf{R} . It is trivially orthogonal because they result from a unitary transformation of the Bloch states, which

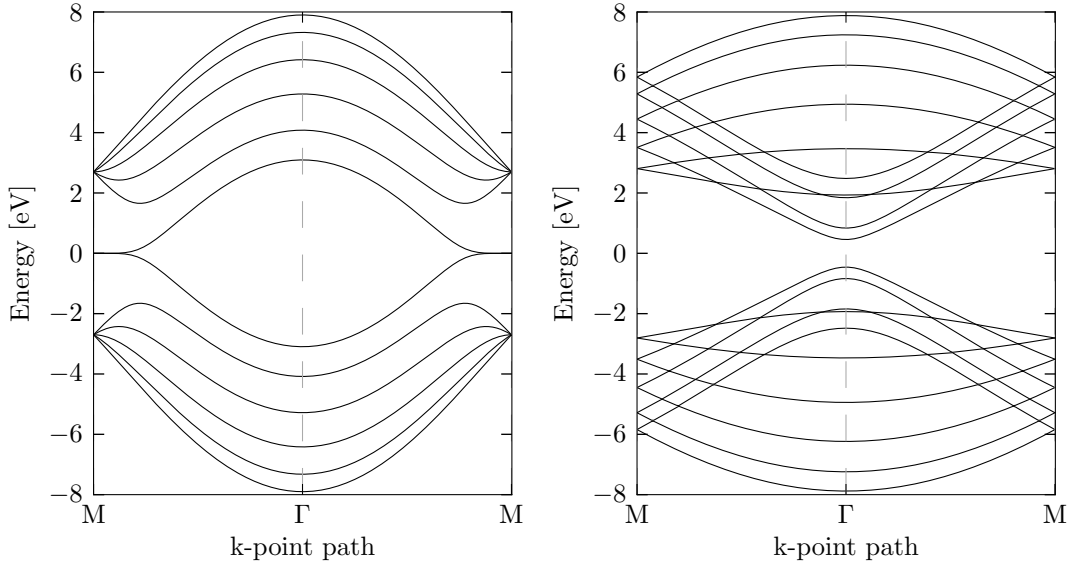


Figure 2.6.: Left: band structure of the π system of a 5-zzGNR, right: band structure of the π system of a 5-aGNR. The zzGNR features flat bands at E_F , which are located at the edges of the ribbon.

are also orthogonal. The process is similar to creating an electromagnetic wave packet by summing over plane waves. U is a unitary matrix which we are free to choose.

2.6.1. Maximally Localized Wannier Functions (MLWF)

Maximally Localized Wannier Functions (MLWFs) describe one way to choose the matrix U . In tight-binding, we want localized basis orbitals in order to associate an electron with a specific atom and to be able to build up system geometries. If the orbital is maximally localized, the number of non-negligible matrix elements to adjacent orbitals will probably also be small. Such a localized orbital is also a "bridge" to atomic orbitals and helps us understand the character of chemical bonding.

The localization of an orbital is measured using the spread Ω , the sum of the orbital variances:

$$\Omega = \sum_n \left[\langle w_{n0}(\mathbf{r}) | r^2 | w_{n0}(\mathbf{r}) \rangle - |\langle w_{n0}(\mathbf{r}) | \mathbf{r} | w_{n0}(\mathbf{r}) \rangle|^2 \right] \quad (2.6)$$

This can be split up into a term $\tilde{\Omega} = \Omega_D + \Omega_{OD}$ (diagonal and off-diagonal in the WF basis) which depends on U and one that does not, Ω_I :

$$\Omega = \tilde{\Omega} + \Omega_I$$

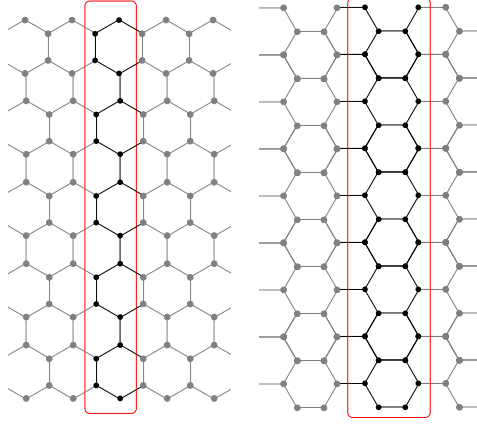


Figure 2.7.: Part of a zigzag graphene nanoribbon (left) and its unit cell (red); part of an armchair graphene nanoribbon (right).

$$\begin{aligned}\Omega_I &= \sum_n \left[\langle w_{n\mathbf{0}}(\mathbf{r}) | r^2 | w_{n\mathbf{0}}(\mathbf{r}) \rangle - \sum_{\mathbf{R}m} |\langle w_{m\mathbf{R}}(\mathbf{r}) | \mathbf{r} | w_{n\mathbf{R}}(\mathbf{r}) \rangle|^2 \right] \\ \Omega_D &= \sum_n \sum_{\mathbf{R} \neq \mathbf{0}} |\langle w_{n\mathbf{R}}(\mathbf{r}) | \mathbf{r} | w_{n\mathbf{R}}(\mathbf{r}) \rangle|^2 \\ \Omega_{OD} &= \sum_{m \neq n} \sum_{\mathbf{R}} |\langle w_{m\mathbf{R}}(\mathbf{r}) | \mathbf{r} | w_{n\mathbf{R}}(\mathbf{r}) \rangle|^2\end{aligned}$$

For a given set of Bloch states, the MLWF procedure minimizes the sum of the orbitals variances Ω w.r.t. U . The minimization consists of two sequential parts: disentanglement and Wannierization.

The disentanglement procedure decides if a Bloch state will be used in the unitary transformation from Bloch states to Wannier orbitals or not. Because of the unitarity, only as many states per k-point can will be used as there are resulting Wannier orbitals.

If the calculation shall result in N Wannier orbitals, the disentanglement procedure finds a $N \times K$ linear transformation for every k-point that transforms the K Bloch states of that k-point into N Bloch states, so that the part of the spread which does not depend on U , Ω_I , is minimal. If there are N bands within the outer energy window, all bands are used, and the disentanglement procedure is not necessary.

The crucial feature of the disentanglement procedure is that it finds those parts of the band structure which can be combined linearly to a set of orbitals (with a given orbital number N) which minimize Ω . Consider graphene, whose band structure consists of three major parts (see Fig. 2.8): a) the σ system (bottom three bands) b) the π system (bands 4-5) and c) bands well above E_F which are not relevant for conductance (grey in Fig. 2.8). By defining the energy window of eligible states and the number of Wannier orbitals (two), the disentanglement procedure automatically picks the π and the π^* band.

After the disentanglement procedure, there are N Bloch states per k-point ($=N$ bands) left. The wannierization procedure finds U to minimize the total spread Ω (specifically, the part $\tilde{\Omega}$ that depends on U). The result will be the matrix U , which can be used to calculate the Hamiltonian matrix in the localized basis as well as the real-space representation (if the real-space representation of the Bloch orbitals is known).

Graphene has the nice feature that only two orbitals are necessary to describe (most of) the π system. This is because the Hamiltonian matrix elements between the σ and π system are all zero, thus, three orbitals describe the σ bands, and two orbitals describe the π bands. This is not generally the case: If there are more bands within the outer energy window than result orbitals, some bands will be described well, others will not, even with a fully converged calculation.

2.6.2. Tight-binding fit vs. Wannier orbitals

Wannier orbitals differ from the "traditional" tight-binding fitting routine as follows:

- Wannier orbitals contain the exact same information as the Bloch states. Fit tight-binding (normally) only contains part of the information. It follows that Wannier orbitals are as good as the tight-binding approximation can ever get, but the parameter set is much bigger. The amount of memory and processor resources can be reduced by creating a model based on fewer fit parameters which reproduces a selected set of properties of the original Bloch states (e.g. behavior around E_F).
- Wannier orbitals have a real-space representation. Tight-binding parameters usually only reproduce the band structure, and their basis orbitals don't have a real-space representation. Even their center is unknown.
- Fitting tight-binding orbitals implicitly assume the symmetry of atomic orbitals. Wannier orbitals can have their center between atoms.
- For a fitting procedure, one needs a metric to measure the distance between band structures. For systems with many bands, its minimization can range between messy and impossible. This problem is completely avoided using Wannier orbitals.

2.6.3. Choice of energy, k-points and guess orbitals

The Wannierization procedure has several parameters which influence the convergence speed as well as the results.

There are two energy windows needed as input for an MLWF calculation, illustrated in Fig. 2.8.

- The *outer energy window* defines the energy range in which Kohn-Sham orbitals are considered to be used in the transformation. All states which lie outside this window are completely disregarded. A state within the window will be used if it leads to a minimization of the spread Ω . All relevant bands must be within this window. More bands than resulting orbitals may exist there. With a well-chosen

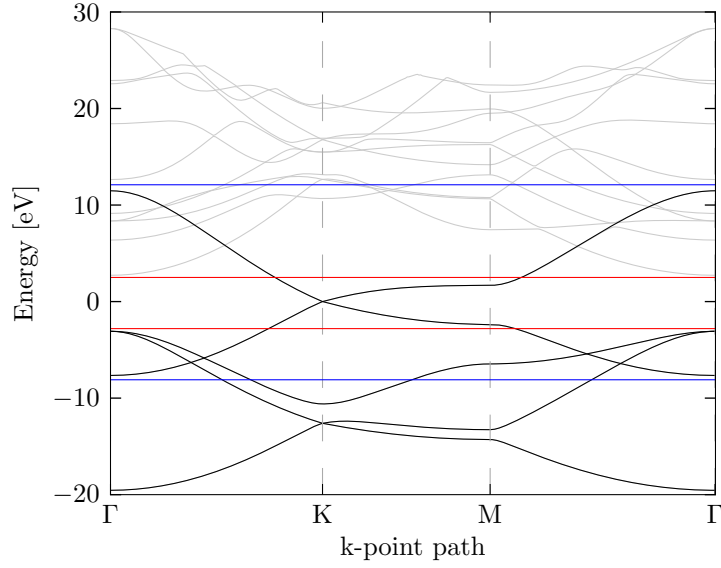


Figure 2.8.: Outer (blue) and inner (red, "frozen") energy windows for the π bands of graphene. In this case, the frozen energy window encapsulates the energy range which is exclusively occupied by the π bands. The outer energy window encapsulates the energy range which is non-exclusively occupied by the π bands.

set of initial guess orbitals, the MLWF procedure will automatically select the relevant bands.

- The *inner/frozen energy window* defines the energy range in which all Kohn-Sham orbitals must be used. Mandatory bands which are to be kept are within this window. Bands which are to be disregarded must not be there. The frozen energy window must lie within the outer energy window.

If a band that is to be reproduced by Wannier orbitals is not completely within the outer energy window, the disentanglement procedure does not converge.

The extent of the outer and frozen energy window greatly influences the resulting Wannier orbitals.

A set of guess orbitals which resembles the expected results significantly increases the convergence speed (although it does not influence the result). The valence orbitals of the atom type are (obviously) a good start. Additionally, there will be electron density at the bonding lines.

2.6.4. Tight-binding parameters

The MLWF procedure gives the unitary transformation matrix U as a result. It describes the transformation from KS Bloch states to localized orbitals. Since each KS state has an

energy, the Hamiltonian matrix in the KS basis E is diagonal and has the KS energies as diagonal entries. The Hamiltonian in the Wannier orbital basis can be calculated by applying the transformation U on the diagonal Kohn-Sham Hamiltonian H_{KS} . The entries of the resulting matrix H_{TB} are on-site and hopping matrix elements between the Wannier orbitals and can be used for tight-binding.

Because of the lattice symmetry, it is sufficient to specify the hopping matrix elements from the atoms within one cell ("main cell") to all other cells in the vicinity.

2.6.5. Real-space representation

Using the transformation matrix U , the real-space representation of a Wannier orbital can be obtained from the real-space representation of the Kohn-Sham orbitals.

Tight-binding does not require orbitals to be necessarily localized at an atom. It can be practical to use orbitals which are delocalized around tens or hundreds of atoms.

2.6.6. Accuracy of band selection and band reproduction

We can give a few hints when one can expect good reproduction of the desired bands and when one cannot:

- The complete band must be within the outer energy window, otherwise the calculation will not converge.
- If there are fewer destination orbitals than bands in the outer energy window, the disentanglement procedure will select the bands. This will work perfectly if the states in the bands you want to extract do not interact (i.e. the Hamilton matrix elements are zero) with the other bands (like the graphene σ and π system, which are decoupled by symmetry). In general, they do interact, and the description will result in bands which are not completely accurate.
- The MLWF procedure yields poor results if there are bands with the same orbital character in the outer energy window as the bands one wants to describe. They are not automatically disregarded because they actually contribute to the minimization. E.g., the π system of a graphene ribbon with 10 atoms per unit cell has 10 bands. It can be described using 10 p_z -like Wannier orbitals. If the outer energy window contains no other bands which have p_z characteristics, this works perfectly. However, if the size of the outer energy window is increased, there may be other bands with p_z characteristics, which contribute to the minimization and thus distort the description of the π system. To conclude, the outer energy window should be chosen as small as possible.

2.7. Building block system for tight-binding parameters

Tight-binding is based on the assumption that parameters, derived from one specific system configuration (e.g. infinite crystal), also work for other, similar systems. In

the context of the nearest-neighbor approximation, this makes sense: it's unlikely that orbitals which are localized on distant atoms interact, thus, the hopping parameters for a silicon atom which lies in the middle of a grain of sand will be the same as for a silicon atom within an infinite crystal. However, this assumption is invalid if the local chemical environment of an atom is different from the initial system, e.g. a missing atom, a substitution atom or an adsorbed atom or an edge. Using the tight-binding parameters of an infinite crystal for those systems (which is the usual approach) leads to quantitatively wrong results. We propose that parameters for different regions in the tight-binding geometry come from different ab-initio calculations. E.g., for a graphene nanoflake, most of the atoms are "bulk" atoms, whose parameters will come from an infinite crystal calculations, but at the edges, parameters from an ab-initio calculation which included edges will be used (e.g. a nanoribbon).

After creating a set of building blocks which describe different defects, larger systems which feature all of those defects can be calculated with the same computational efforts, but at much higher accuracy.

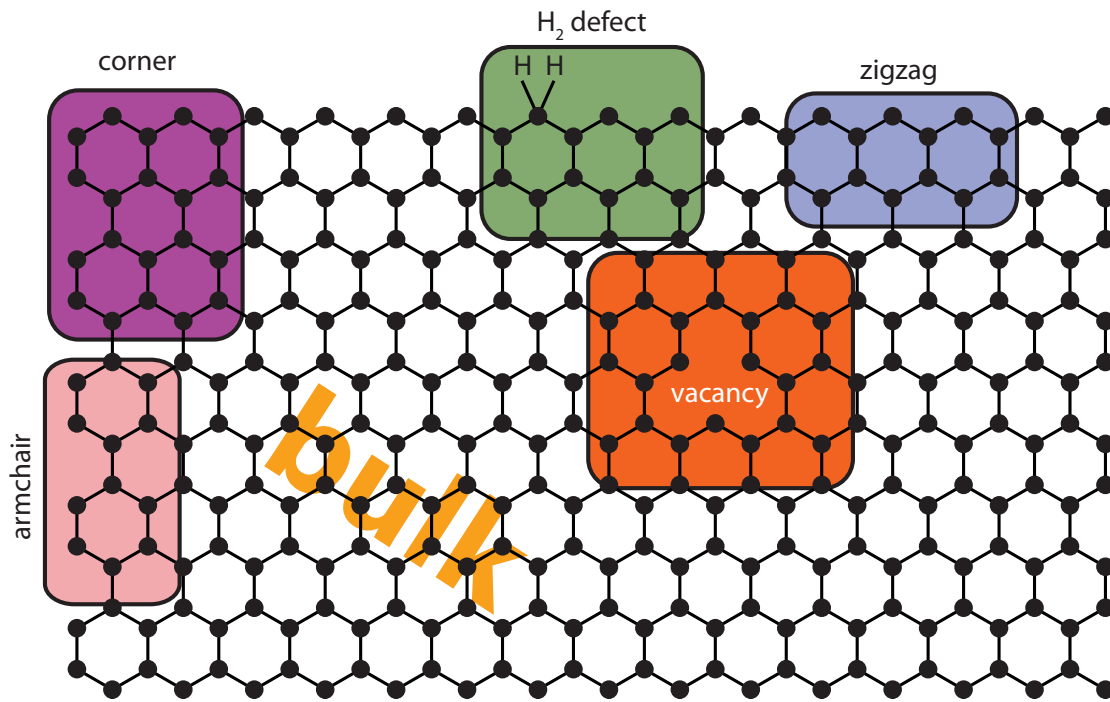


Figure 2.9.: Schematics of building blocks, illustrated for graphene. Every block encapsulates a common defect and can be re-used in combination with bulk tight-binding parameters.

3. Infinite graphene sheets

The case of the infinite graphene crystal is the easiest one to calculate; we will evaluate the performance of the MLWF procedure, compare it to the traditional fitting tight-binding scheme and then work our way towards more complicated structures.

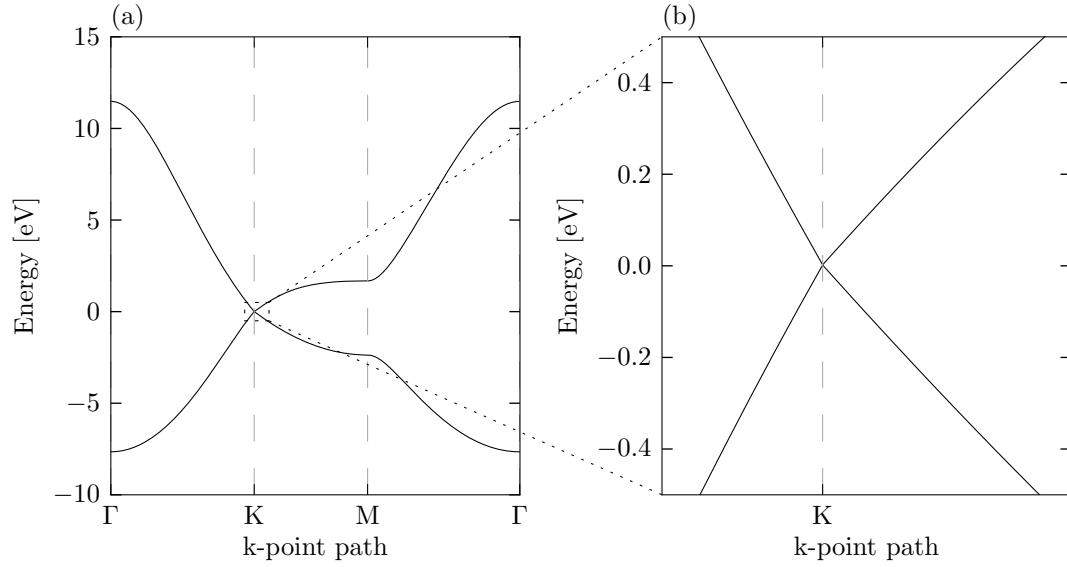


Figure 3.1.: DFT band structure of the graphene π -system (a) along Γ KM Γ (b) enlarged view around the K point showing the linear behavior.

3.1. Nearest-neighbor parameterization

3.1.1. Fitting procedure to DFT band structures

For determining tight-binding parameters, we consider the band structure of the system. We reproduce the DFT-LDA band structure using a tight-binding calculation with fit parameters. The assumption here is that the tight-binding Hamiltonian, which belongs to a single-particle Schrödinger equation, can reproduce the single-electron energies of a many-electron calculation. The tight-binding Hamiltonian uses an implicit mean-field description to account for the effect of the other electrons. This follows the strategy behind the Kohn-Sham ansatz of DFT which assumes that the interacting system can

be described by a noninteracting system (which is a single-particle problem) with an effective potential.

The algorithm is as follows:

- Choose a set of tight-binding parameters
- Construct the tight-binding Hamiltonian as a function of the wave vector \vec{k}
- Solve the eigenvalue problem for every \vec{k} along a certain path in the Brillouin zone
- Compare this tight-binding band structure with the DFT results using a distance function/norm.
- Repeat until the norm reaches a minimum.

We used the Levenberg-Marquardt algorithm [18] for the minimum search.

Because the basis set used in tight-binding is not complete, it is obvious that not the entire band structure can be reproduced. The energies that correspond to wave functions which cannot be described by the restricted basis set will show large discrepancies. The bands that cannot be described by any choice of tight-binding parameters are disregarded in the minimum search.

The error can be weighed according to relevance. A possible choice for a band structure fitting distance is the 1-norm, which takes the form of

$$w = \frac{1}{N} \sum_{n,m} g_{mn} |a_{mn} - b_{mn}|. \quad (3.1)$$

n is the band index, m is the point index on the chosen path through the Brillouin zone, g_{mn} is a positive weighing factor (if all data points are equally important, $g_{mn} \equiv 1$), a_{mn} and b_{mn} are the DFT and tight-binding band structure data points, respectively. N is the number of sample points along the path to make the error of a certain resolution comparable to an other resolution (other value of N).

3.1.2. 1st-nearest-neighbor parameterization

The 1st-nearest-neighbor parameterization has only two parameters: ε and t . ε causes a spectral shift which shifts the whole band structure up and down, whereas t is the only parameter defining the shape. It can be directly related to the slope of the Dirac cone at the K point, and through $v_g = \frac{1}{\hbar} \frac{dE}{dk} = \frac{\sqrt{3}}{2\hbar} ta$, to the Fermi velocity.

This parameterization only incorporates the symmetry properties of the system and the Fermi velocity. The determination of the parameters is trivial: $\varepsilon = E_F$, and t can be related to v_F which is measured or calculated. The values used in Fig. 3.2 are $\varepsilon = 0$ eV and $t = -2.7$ eV.

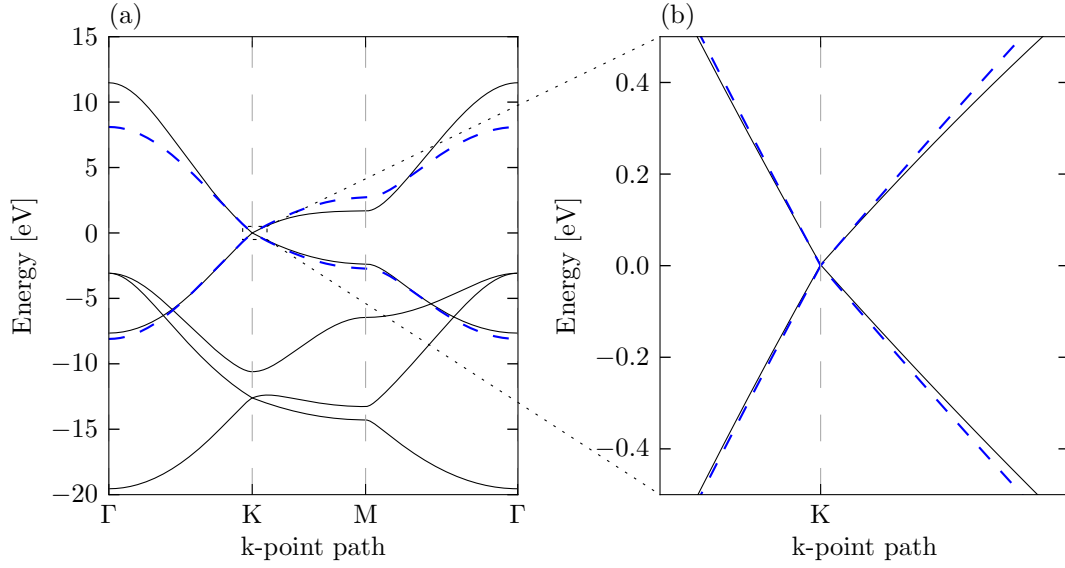


Figure 3.2.: 1st-nearest-neighbor tight-binding (blue) and DFT band structure of graphene (black) (a) along Γ KM Γ (b) enlarged view around K .

3.1.3. 3rd-nearest-neighbor parameterization and higher

The 3rd-nearest-neighbor parameterization correctly describes a "trigonal warping" effect of the Dirac cone at K towards higher energies. Also, the overall agreement with the DFT band structure is better. The Slater-Koster hopping parameters don't have an obvious physical interpretation as in the 1st-nearest-neighbor case.

The arbitrary choice of the minimization norm plays a significant role: it's not possible to reproduce the complete π and π^* band using 3rd-nearest-neighbor parameterization, but we can choose which part to describe better by using the appropriate norm. Set 1 (see Fig. 3.3 and Fig. 3.4) describes the π band correctly, whereas set 2 produces a symmetric band structure. For quantum conductance calculations, the relevant range is described equally well.

Note that, although the parameters depend on the norm, the best fit for a given norm is unique and always converges to the same parameters for different starting guesses.

#	Set 1 [30]	Set 2 [13]
ε	1.0797	-0.126
1	-3.4727	-3.145
2	0.3616	-0.042
3	-0.2376	-0.35

Figure 3.3.: Comparison of two different sets of 3rd-nearest-neighbor parameters (see Fig. 3.4). Units in eV. The index denotes the nearest neighbor group.

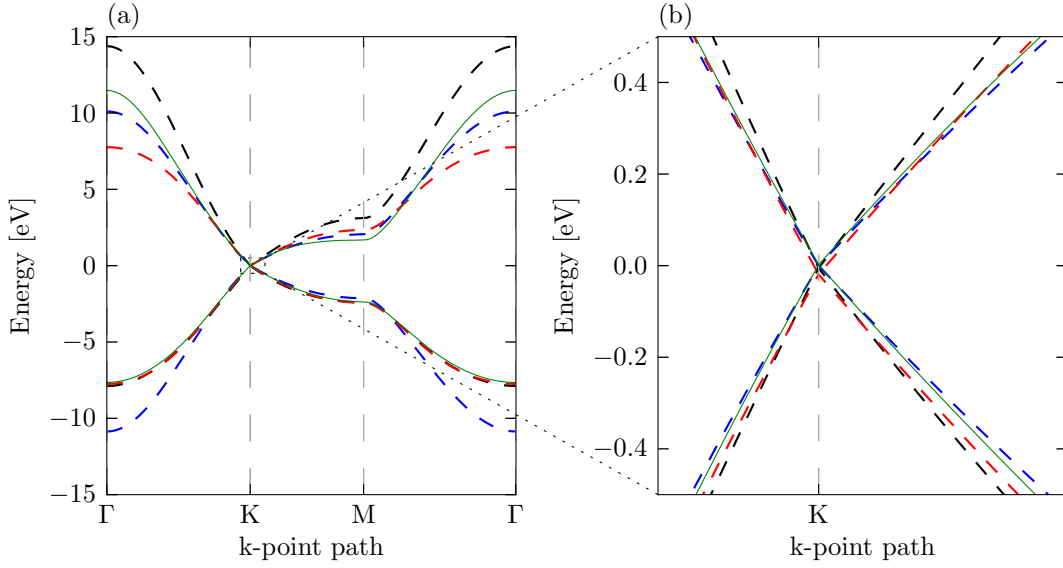


Figure 3.4.: Comparison of four different parameterisations of the graphene π system: 3rd-nearest-neighbor set 1 (black), 3rd-nearest-neighbor set 2 (blue), 5th-nearest-neighbor [30] (red) and DFT (green) (a) along Γ KM Γ (b) enlarged view around K .

3.1.4. Computational effort

Due to symmetry, the number of parameters for a n^{th} -nearest-neighbor parameterization is $n + 1$. The computational effort, though, grows with a higher power of n because the number of matrix elements between the reference cell and its neighbor cells grows with n^2 (because of the area covered). Each hopping matrix element (i.e. all connections between the atoms in the reference cell and the other cells as depicted in Fig. 2.1) corresponds to one entry per row in the Hamiltonian matrix; e.g. a matrix derived from the 1st-nearest-neighbor parameterization has 4 nonzero entries per row. The performance of the algorithm used for inversion or diagonalization of the Hamiltonian matrix usually depends on the number of nonzero entries per row.

3.2. Parameterization using MLWFs

The MLWF procedure does not depend on the choice of a norm between the approximated and the DFT band structure. However, we can choose the number of resulting Wannier orbitals and an energy window where the participating Bloch states will be chosen from. Depending on how the bands in the energy window "mix" with the bands outside or reaching into the window, the desired bands will be reproduced perfectly or not.

For graphene, there are two different scenarios:

- Parametrize the π and the σ system with five Wannier orbitals. The result will be two p_z -like orbitals for the π system and three sp^2 hybrids for the σ system. The disentanglement procedure will automatically choose the five relevant bands from the energy window which must be large enough to contain all of them.
- Parametrize the π system with two Wannier orbitals, resulting in the same two p_z -like orbitals as the previous scenario. The disentanglement procedure will also choose the relevant bands (π , π^*) from a window that contains both of them and will disregard the others, including the σ bands.

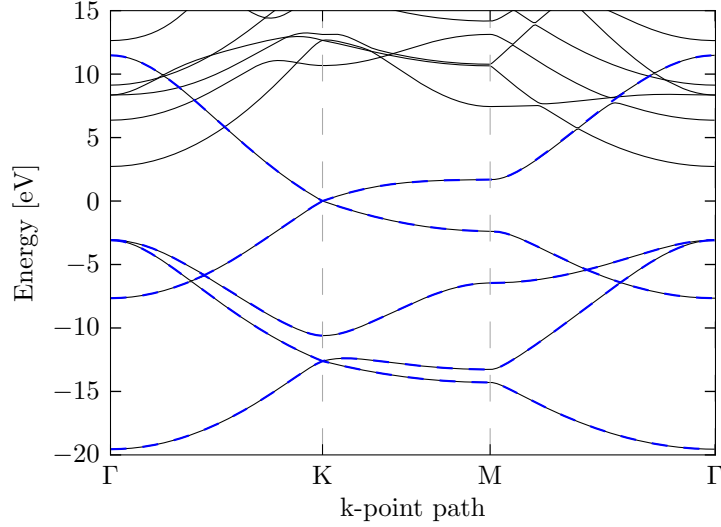


Figure 3.5.: Graphene DFT band structure (black) and derived Wannier orbital band structure (blue) for the σ and π system.

There is an important difference between the MLWFs and tight-binding orbitals for the σ system. Using a Slater-Koster parameterization, there are four orbitals per atom, which leads to four occupied and four virtual bands. The first virtual band is the π^* band, but the other three virtual bands don't describe any of the other DFT virtual orbitals because the latter ones are not localized. Thus, Slater-Koster tight-binding needs eight orbitals to describe five bands. The Wannier orbital parameterization, on the other hand, uses only three sp^2 -like orbitals (specifically, the positive linear combinations of the atomic sp^2 -orbitals) for the σ system – there are no virtual partners for those bands.

In addition to standard tight-binding, the MLWF procedure results in a real-space representation of the basis orbitals as well as hopping matrix elements (see Fig. 3.10) which can be used for tight-binding.

The initial guesses (Fig. 3.6) for the p_z -like orbitals are, unsurprisingly, two p_z -orbitals, sitting on the carbon atoms. For the σ system, two possible choices lead to equally good convergence: a) sp^2 hybrid orbitals on every other carbon atom or b) one s -orbital at every half distance point between two neighboring carbon atoms (see Fig. 3.6). Both variants a) and b) feature three orbitals. The outer and frozen energy windows (see Fig.

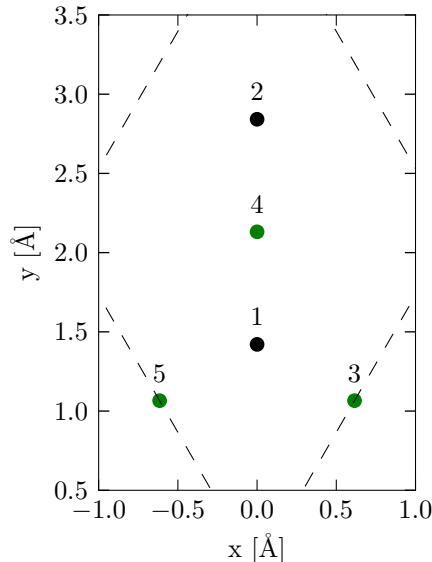


Figure 3.6.: Centers of gravity of the initial guess orbitals for one unit cell of graphene (black dots: p_z -orbitals, green dots: s -orbitals – see Table 3.9 for the orbital types and positions)

2.8 for graphene) should be chosen so that they closely encapsulate the desired bands to maximize the convergence speed. The convergence itself depends on the right choice of the upper window border, because there may be bands which have p_z symmetry. Most of the bands, though, are free particle-like and don't contribute to localized orbitals.

The MLWF procedure does not allow to set the number of hopping neighbors. It just minimizes the spread, and the resulting hopping matrix elements are a result of this optimization process. As shown in Fig. 3.7 and Fig. 3.8, the matrix elements above the 10th nearest neighbor group can be safely set to zero without changing the band structure. Neglecting hopping elements between closer atoms change the band structure visibly (see Fig. 3.8).

The real-space representation of the basis set (Figs. 3.11, 3.12, 3.9) enables us to see where the conduction actually takes place (namely, in the π system). The sp^2 -orbitals (a positive linear combination of the atomic sp^2 -orbitals, to be precise) illustrate the chemical bonding of graphene.

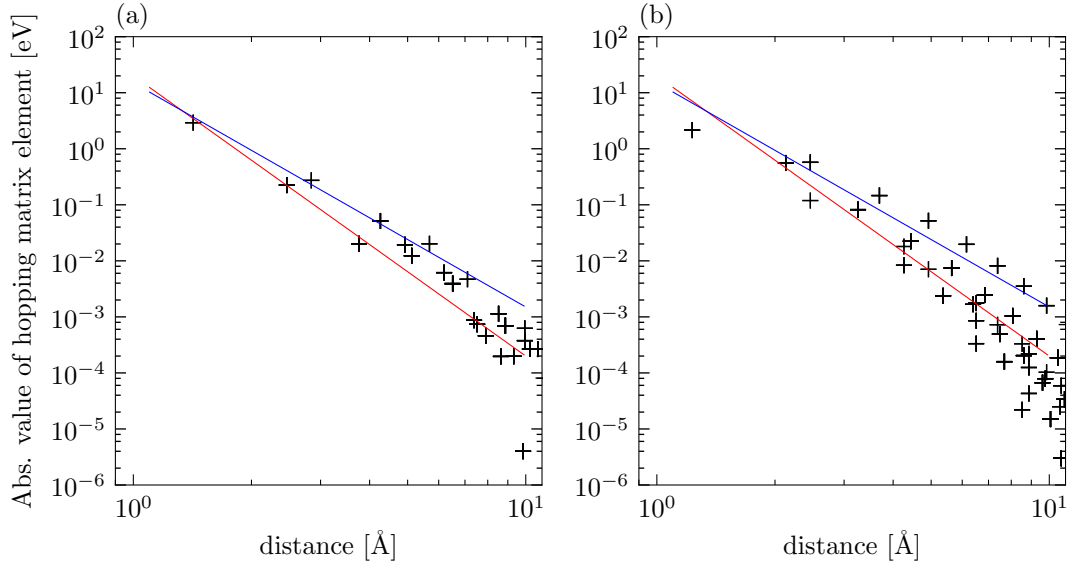


Figure 3.7.: Absolute value of the hopping matrix elements depending on the distance between the orbitals (a) π orbitals (b) σ orbitals). The blue and the red curve are polynomials of degree -4 and -5.

3.3. Conclusions

We have shown that the π and σ systems of graphene can be described accurately using MLWFs in their full energy range with five orbitals (Fig. 3.5). This is in contrast to nearest-neighbor tight-binding parameterisations obtained from fit procedures, which need eight orbitals and fail to describe the full π system (Fig. 3.4). However, a large parameter set (more than 10 neighbor groups, see Table 3.10) needs to be used for transport calculations to describe the electronic structure at the Fermi energy.

The MLWFs have a real-space representation that describes the orbitals of the π system as p_z -like orbitals (Fig. 3.11) and the orbitals of the σ system (Fig. 3.12) as positive linear combinations of atomic sp^2 hybrids. The correct choice of the outer and frozen energy window (Fig. 2.8) is crucial for the convergence of the MLWF procedure.

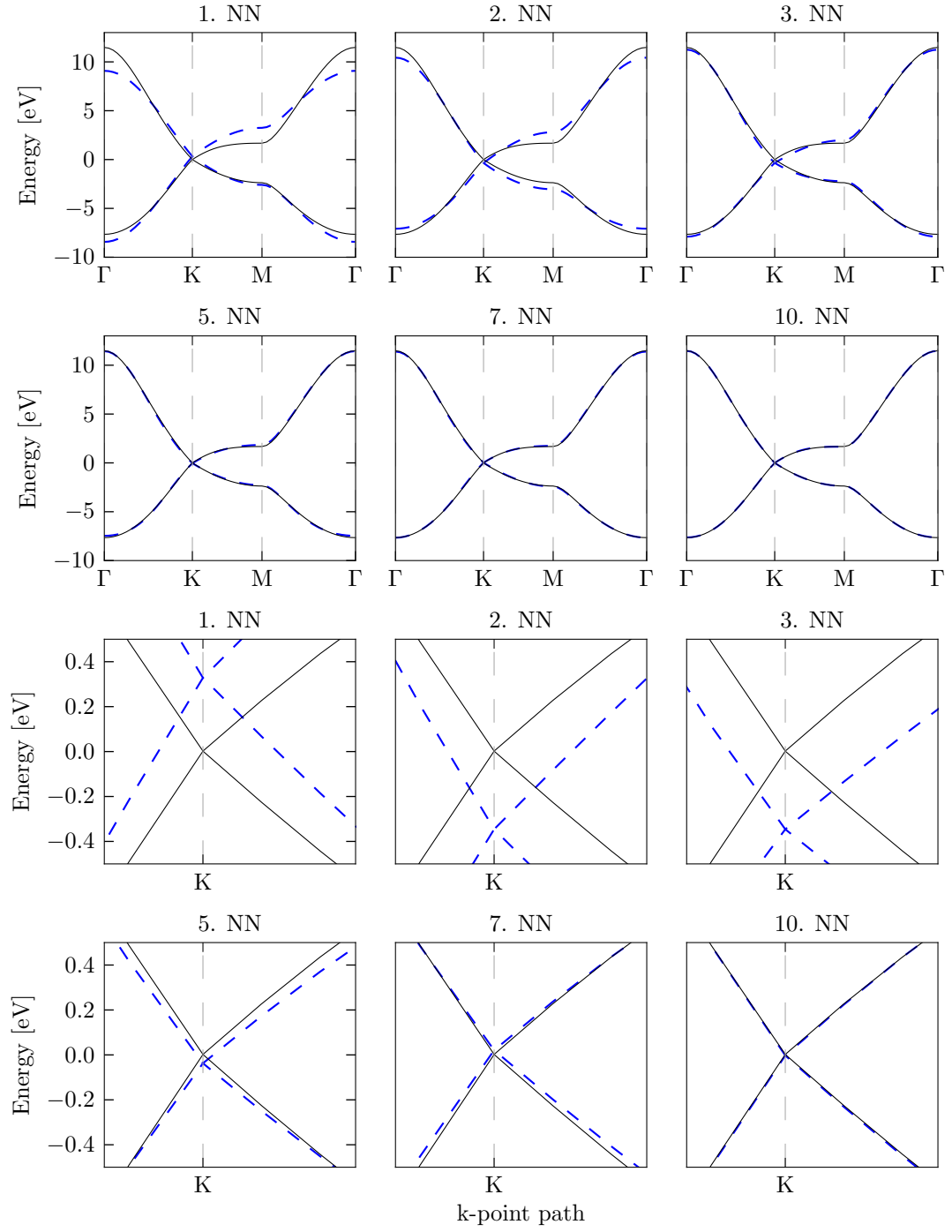


Figure 3.8.: DFT (black) and Wannier orbital (blue) band structure for various hopping parameter cutoff radii/nearest neighbor groups. The lower six panels are enlarged views around K , showing that a large cutoff radius (compared to 3rd nearest neighbor TB) is necessary for a description suitable for transport calculations.

#	type	x	y	z	spread
1	p_z	0	1.42085	0	0.895
2	p_z	0	2.84171	0	0.895
3	sp^2	0.61525	1.06564	0	0.603
4	sp^2	0	2.13128	0	0.603
5	sp^2	-0.61525	1.06564	0	0.603

Figure 3.9.: Centers of gravity and spreads (see Eq. 2.6) of the Wannier orbitals in real-space representation. The numbers refer to the positions in Fig. 3.6.

#		#	
ϵ	3.282830e-01	6	-1.938300e-02
1	-2.918915e+00	7	-1.232300e-02
2	2.247330e-01	8	-2.015500e-02
3	-2.728070e-01	9	6.161000e-03
4	2.019100e-02	10	3.925000e-03
5	5.142900e-02		

Figure 3.10.: First ten hopping parameters for the graphene π system, generated by the MLWF procedure (units in eV). The number refers to the neighbor group.

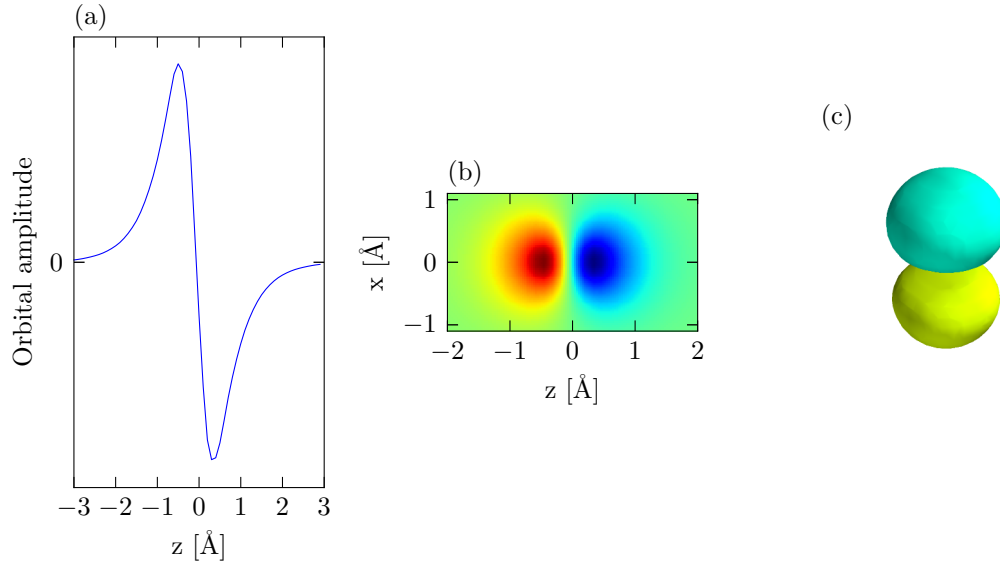


Figure 3.11.: Plots of the p_z -like orbital (Nr. 1 and 2 in Fig. 3.6): (a) wave function along the z -axis (b) on the x - z plane (c) surface plot.

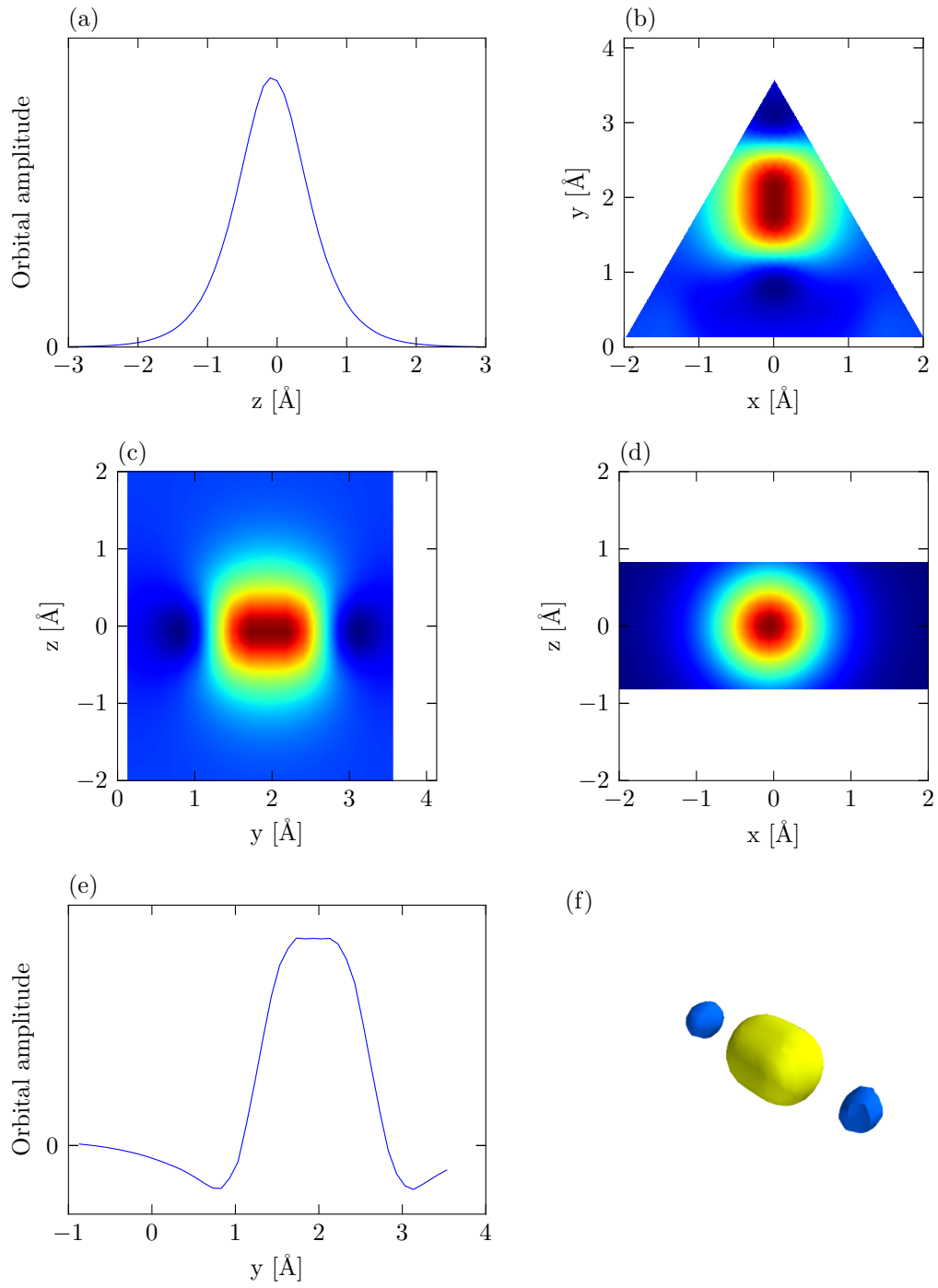


Figure 3.12.: σ -system: (a)-(f) sp^2 orbital (Nr. 4 in Fig. 3.6; Nr. 3 and 5 are copies rotated by 60° in the x - y plane).

4. Defect structures

One of the goals of using Wannier orbitals to create tight-binding parameters is to enhance quality of the description of defects. The proposed procedure goes as follows:

- Do a DFT calculation of the ideal system/bulk material (e.g. infinite graphene crystal). Create the bulk Wannier orbitals.
- Do a DFT calculation of a defect structure within a supercell (e.g. 4 by 4 nm graphene cell with a vacancy). Create defect Wannier orbitals.
- Build up the system geometry by "cutting" a given shape out of the bulk material and use the bulk Wannier parameters.
- Substitute the regions where the defect occurs with the defect Wannier parameters. We call this "parameter mix-in".

There are two assumptions behind this strategy:

- The influence of the defect is local. In tight-binding, this is the case if the non-zero hopping matrix elements are within a certain radius of the orbital. This is in the spirit of the nearest-neighbor approximation and is most likely a good approximation for our purposes.
- The mix-in parameters should connect to the rest of the system in a smooth fashion. While the parameters at the defect are different by construction, the parameters at the border of the substituted area should match the the bulk parameters.

This matching property is very important. It is not a property of the standard MLWF procedure that the boundary (which is physically bulk-like) of a (periodic) supercell has the same Wannier orbitals and parameters as an actual bulk calculation. The minimization of the orbital spread Ω does not guarantee a similarity of orbitals between calculations because the defect may change the situation in an uncontrolled manner. The physics of the bulk-like boundary is, of course, the same as in the bulk, but the Wannier orbital description might still differ. Matching of mix-in cell border parameters with bulk parameters could be enforced by imposing a boundary condition on the MLWF procedure so that the outer border of the supercell has fixed Wannier orbitals which participate in the calculation, but are not varied during the minimization procedure.

In the following, the MLWF procedure for the supercells will be done without any modifications to the MLWF algorithm.

4.1. Zigzag graphene nanoribbons

A graphene nanoribbon has a very strong defect: the ribbon edge. The usual tight-binding parameterization for a ribbon is done by cutting out a ribbon out of an infinite graphene sheet, i.e. using only the bulk parameters and pretending that the cut-off carbon atom next to the outermost edge atom is missing. This results into a surprisingly good description of a real graphene nanoribbon whose edges are passivated with hydrogen.

In the following, we show a procedure how to increase the accuracy of the band structure description by doing a parameter mix-in of the ribbon edges, including the possibility of edge relaxation, which will especially improve the description of states around E_F .

4.1.1. DFT calculation

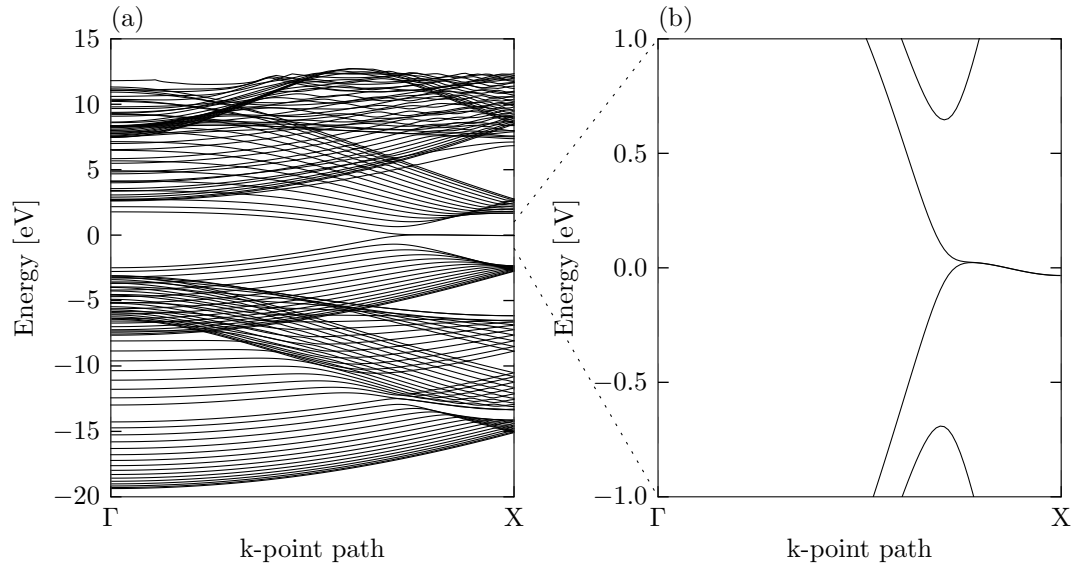


Figure 4.1.: DFT band structure of a relaxed 15-zzGNR (a) along ΓX (b) enlarged view with a rescaled energy axis.

A realistic chemical structure features hydrogen atoms passivating the dangling bond of the outermost carbon atoms (one per edge per unit cell).

In a plane wave DFT calculation with a periodic unit cell, there is not only a periodicity in the ribbon direction (usually x), but also in the other two directions. To eliminate the unphysical interaction between copies of the stripe, there has to be enough distance (vacuum) in y (in-plane perpendicular to ribbon) and z direction (out-of-plane).

In the space between the stripes, there is a number of virtual electronic states with an energy greater than E_F . With increasing cell size, their energy approaches E_F (see Fig.

4.2). For the creation of tight-binding parameters, we need the complete antibonding bands which lie in a range where the aforementioned electron bands accumulate. Thus, the number of bands that need to be included in the DFT calculation grows with increasing box size. On the other hand, as mentioned, the box size in y and z direction needs to be large to avoid interaction; thus, we use a compromise box size of $z=5\text{\AA}$.

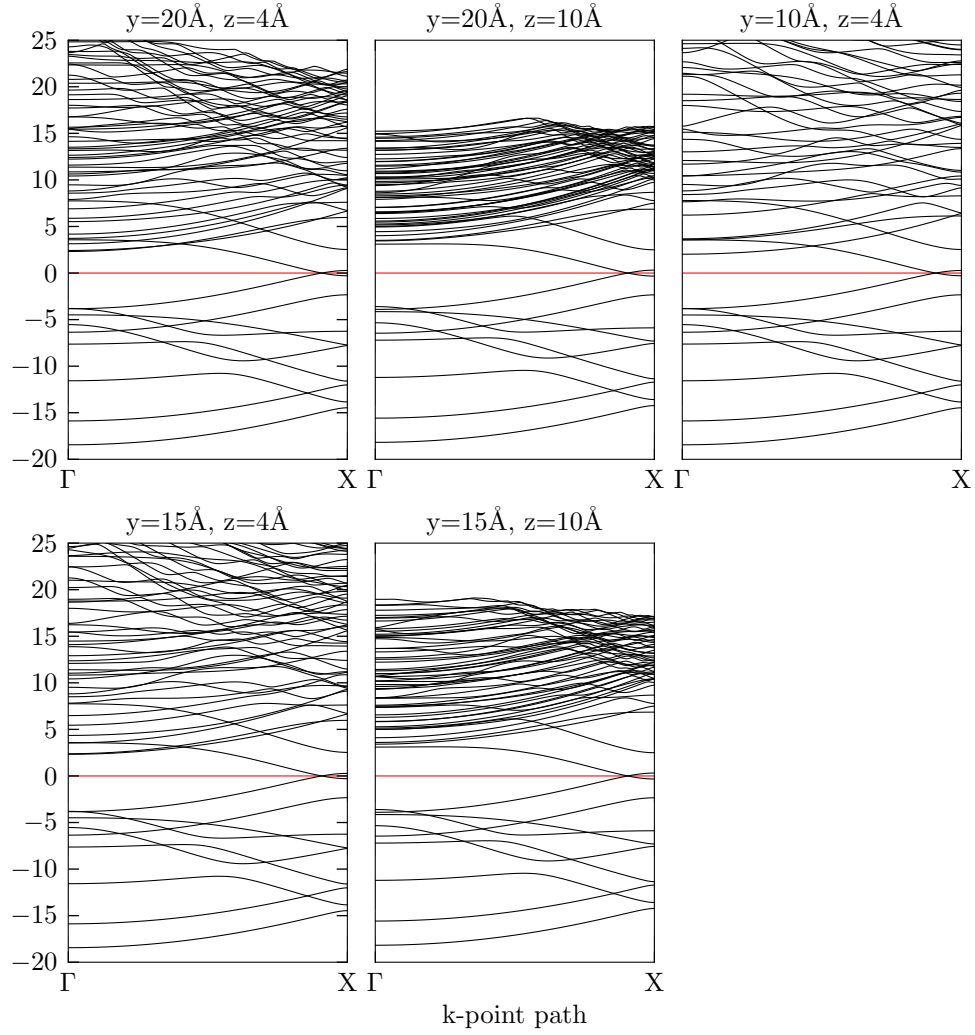


Figure 4.2.: DFT band structure comparison of a 1-zzGNR, running in x -direction, for different box sizes. The red line marks E_F .

4.1.2. Wannier orbitals for a nanoribbon

We use the MLWF procedure to create Wannier orbitals and parameters for a graphene zigzag nanoribbon and analyze the dependence of the parameters on the position within the nanoribbon.

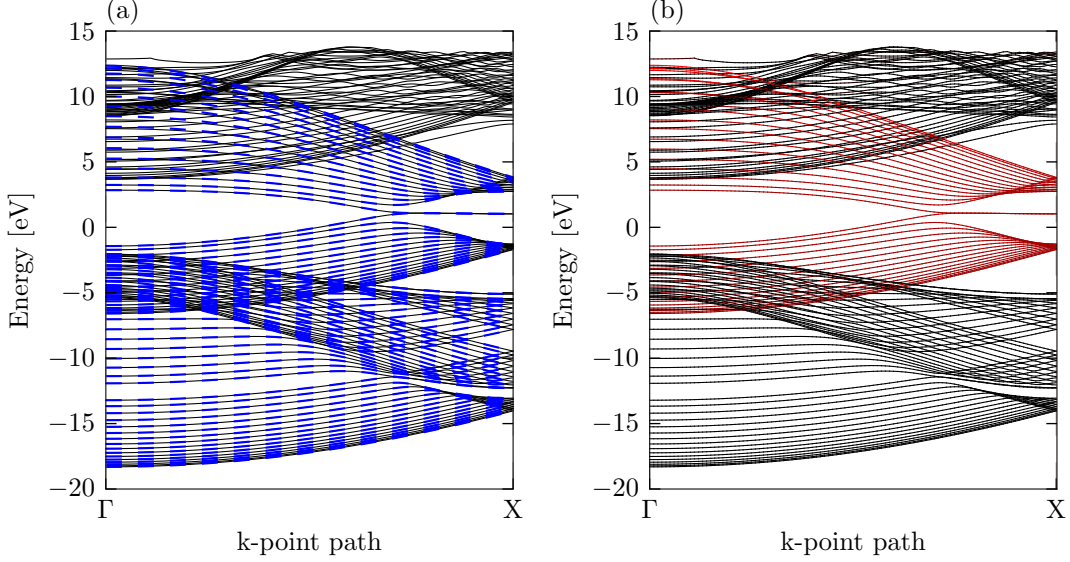


Figure 4.3.: (a) DFT band structure (black) of a 15-zzGNR and the derived Wannier orbital band structure (blue) (b) p_z orbital projection amplitudes of the bands (black: small amplitudes, red: large amplitudes).

Fig. 4.3 shows the DFT band structure of a 15-zzGNR and the derived Wannier orbital band structure. The Wannier band structure reproduces the σ and the π system and ignores the additional bands above E_F . The figure also shows the projection amplitudes of the Kohn-Sham orbitals on the p_z orbitals and illustrates that the MLWF method indeed picks out the bands with p_z characteristics.

The upper boundary of the outer energy window has to be chosen carefully because the DFT calculation shows states which have p_z components in the region above the π^* band. They most probably occur due to poorly converged bands (in the DFT calculation) in the region far above E_F . They must be outside the outer energy window because they would contribute to the minimization of the π system and thus distort those bands.

The upper boundary of the frozen window lies just beneath the energy where the non- p_z bands intersecting with the π^* -system.

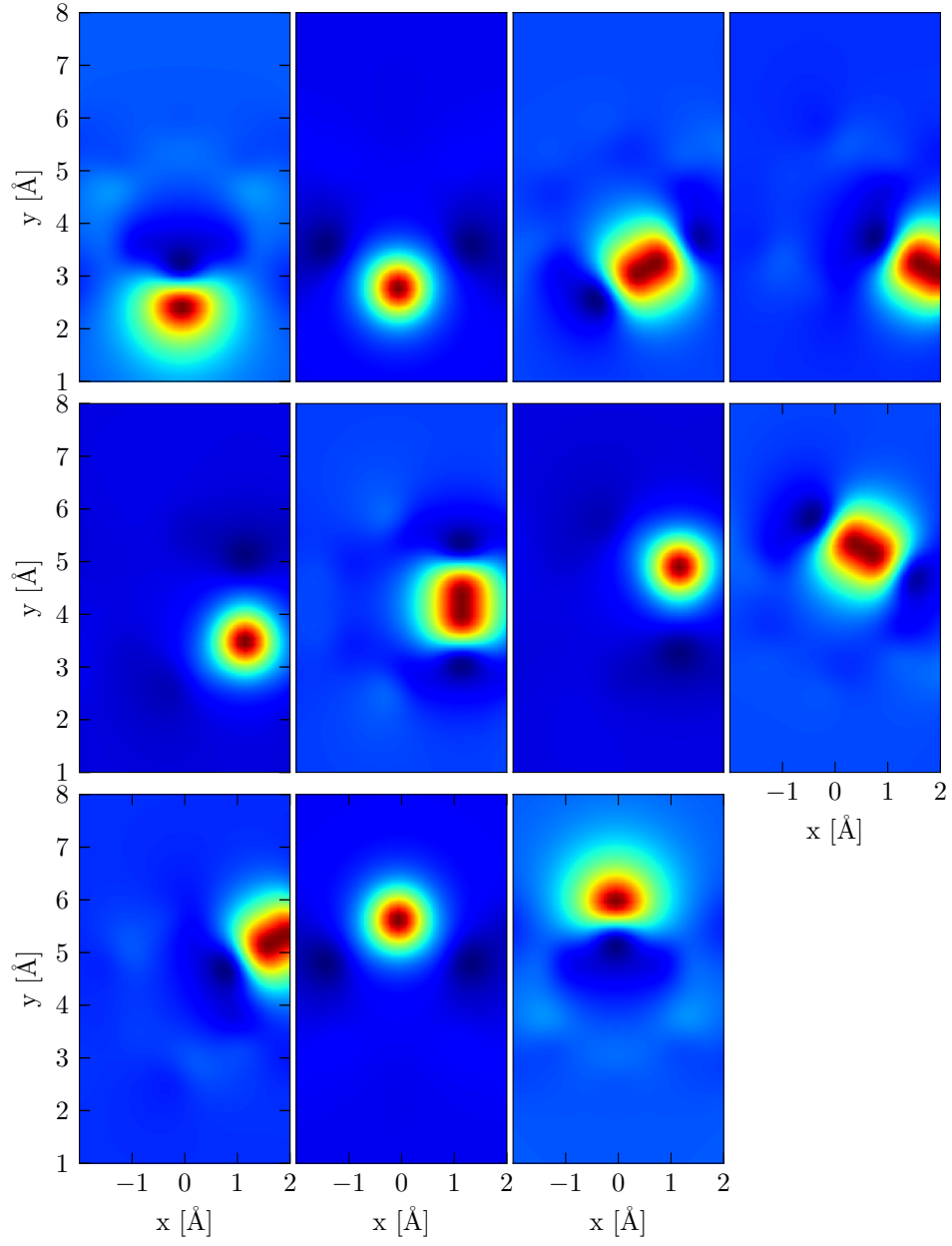


Figure 4.4.: The MLWF Wannier orbitals of a 1-zzGNR; in accordance with Fig. 4.5, from top left to bottom right: Orbitals 1, 0, 6, 8, 2, 7, 3, 9, 10, 4 and 5.

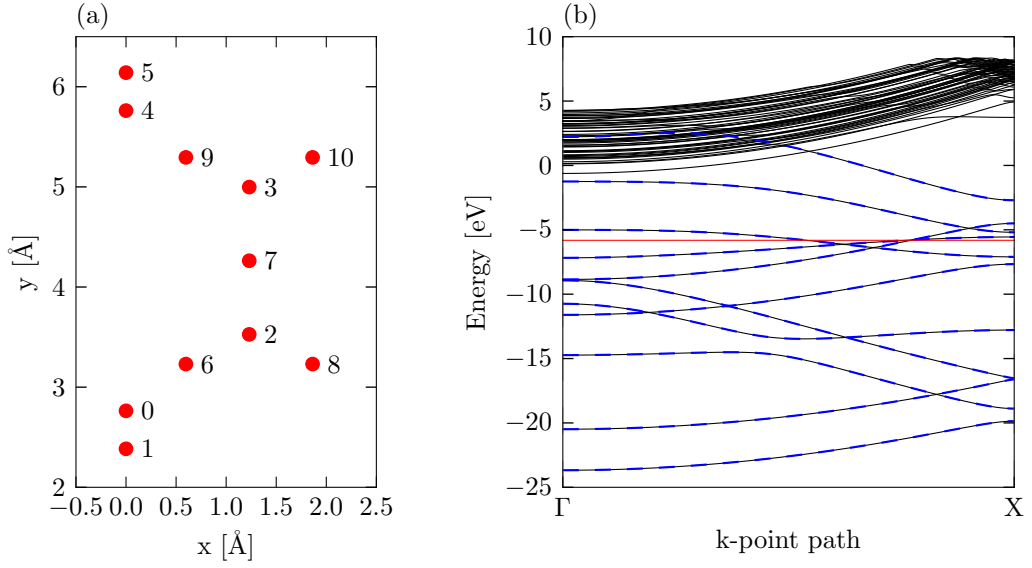


Figure 4.5.: (a) centers of the Wannier orbitals (the index refers to Fig. 4.4) (b) band structure (DFT: black, Wannier orbitals: blue) of a 1-zzGNR. The red line marks E_F .

The real-space representations for the Wannier orbitals in a nanoribbon have the same characteristics as the ones in infinite graphene. The additional hydrogen atoms at the edges result in a p_y -like orbital. Fig. 4.4 shows all orbitals, Fig. 4.5 the center positions.

- The region described by the building block must not be influenced by the width of the nanoribbon, i.e. the edge matrix elements coming from a ribbon calculation must be independent from this width.
- The "bulk" region within the nanoribbon needs to have approximate translational symmetry, and the matrix elements should be identical to the bulk matrix elements.

Fig. 4.6 and 4.7 show the on-site energies of the p_z -like orbitals, dependent on the position, for different nanoribbon sizes. Two qualitatively different patterns emerge (compare e.g. Fig. 4.6, second row vs. fourth row). This is not understood, but we believe that the strongly changing pattern stems from a convergence issue.

The other pattern (from 14 to 30 rings, see especially Fig. 4.7) shows a behaviour which is very suitable for a building block system. The on-site energy in the "bulk" region is uniform. The on-site energies at the edge vary, but in a very similar way if compared between different nanoribbons. Fig. 4.7 shows an enlarged version of the on-site energies of a 20-zzGNR and 15-zzGNR and suggests that the best size for an edge building block includes the outermost 10 atoms.

Unfortunately, the "bulk" on-site energies do not have the same value as the real bulk on-site energy (red line). This is also not understood.

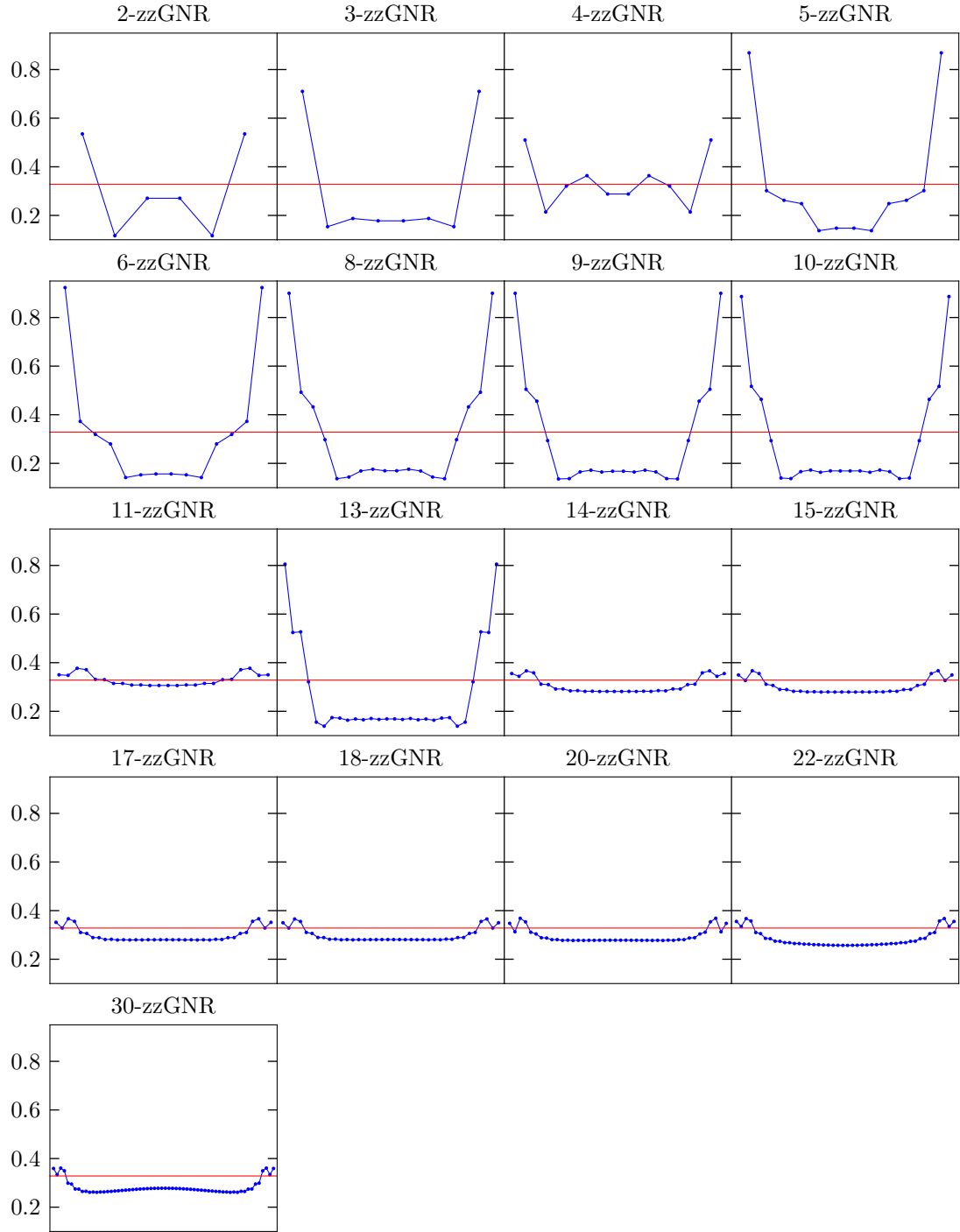


Figure 4.6.: On-site energy of the p_z orbitals, sorted by their position perpendicular to the ribbon orientation. The red line marks the Wannier bulk on-site energy. Units are eV.

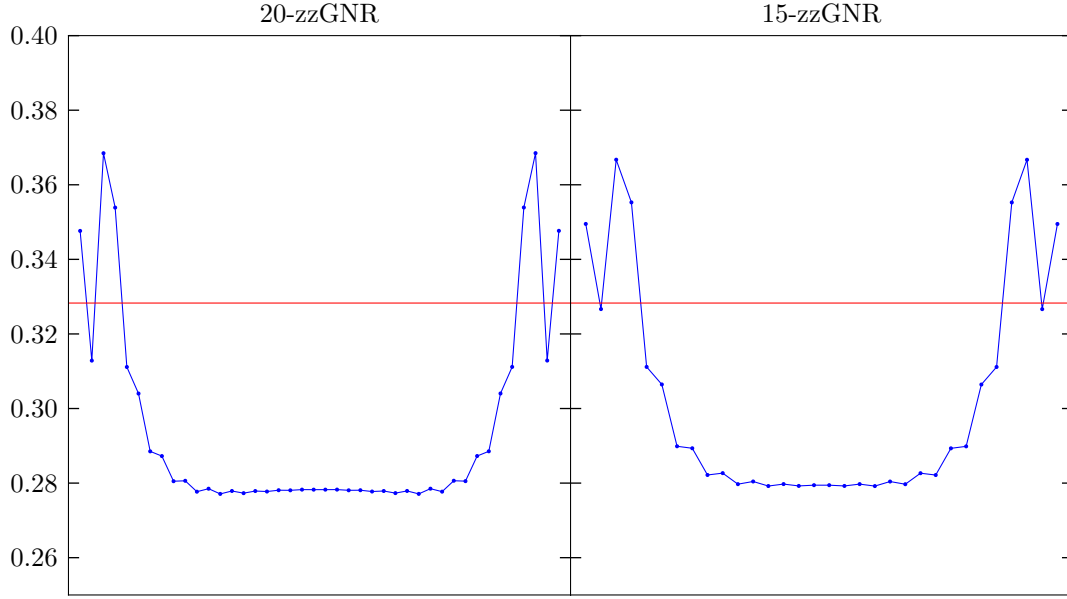


Figure 4.7.: On-site energy of the p_z orbitals along the width of the nanoribbons (enhanced view of Fig. 4.6). The red line marks the Wannier bulk on-site energy. The unit is eV.

4.1.3. Band structure from graphene Wannier parameters

In Fig. 4.8 various nearest-neighbor approximations to the band structure, the original DFT and the Wannier band structure are compared. Note that the Wannier orbital parameters originate from the bulk calculation.

The comparison shows that the DFT band structure is qualitatively well described by all parameterizations, but not quantitatively; in particular:

- The 1st-nearest-neighbor parametrization is inaccurate in every energy regime and lacks a bending of the edge state bands near E_F .
- The 3rd-nearest-neighbor set 2 parameterization is inaccurate in the regime away from E_F and more accurate near E_F . Note that all edge states are below E_F (and thus, filled), which is in contrast to the DFT band structure where only half of the edge states are filled. The set 1 parameterization is completely off.
- The Wannier bulk parameterization is accurate in the regime away from E_F and moderately accurate at E_F , most importantly, the bending of the edge band is much too strong.

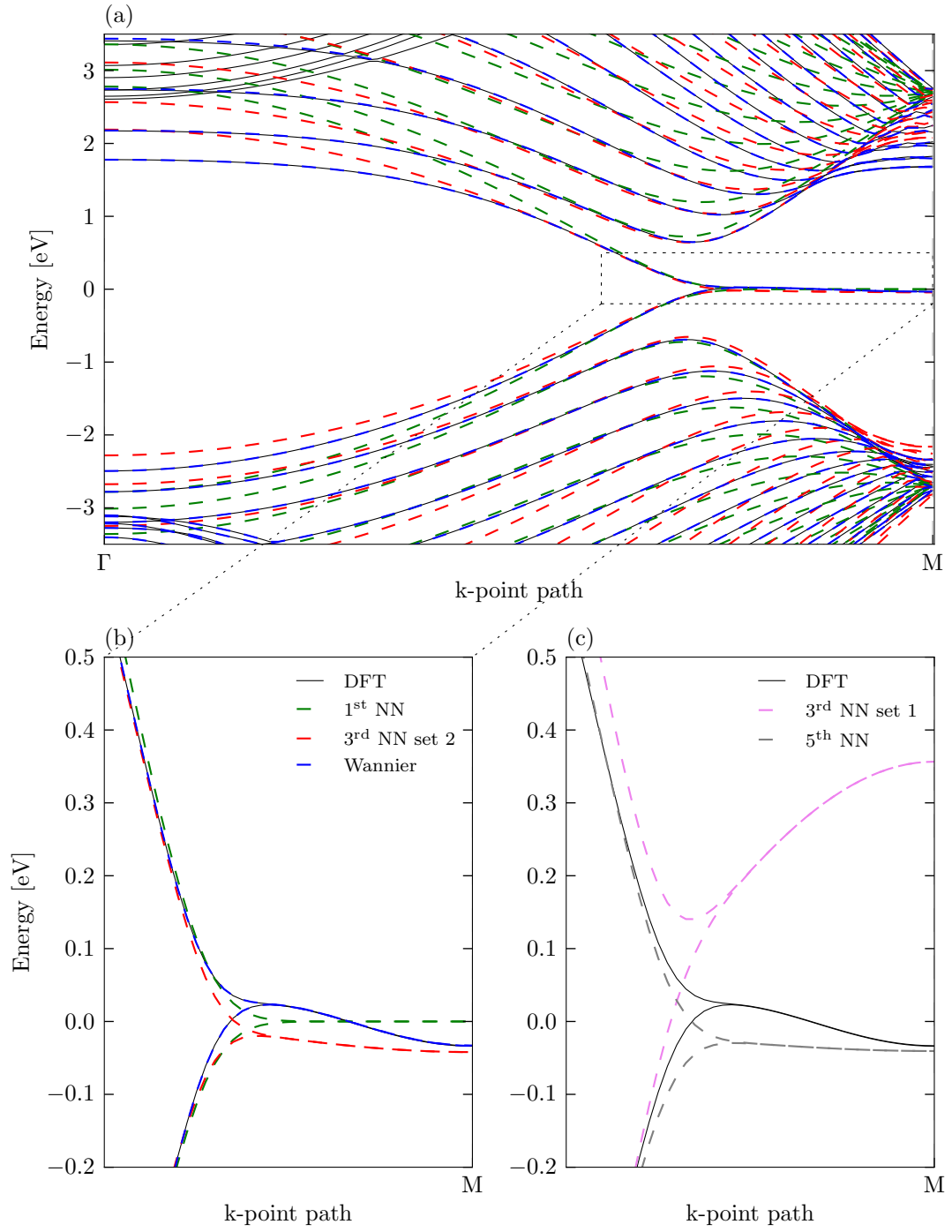


Figure 4.8.: Band structure of a 15-zzGNR. The plots (a)-(c) show different parts of the band structure with different parameterisations in each plot ("Wannier" refers to a Wannier parameterization of the full nanoribbon). (b) shows an enlarged region of (a), while (c) shows the same region, but other parameterizations.

4.1.4. Application of building blocks

We apply the building block principle to a graphene nanoribbon to improve the quantitative description of the band structure. Because the edges are considered as defects, the main error of the tight-binding band structure is expected near the bands around E_F (edge states). As an illustrating example, we will look at a 15-zzGNR.

The following steps are taken:

- DFT calculation of infinite graphene (hexagonal unit cells, 2 atoms) and creation of Wannier orbitals (2 orbitals) for the π system.
- DFT calculation of a zigzag nanoribbon with 15 rings (rectangular unit cell, 32 atoms) in width and creation of Wannier orbitals (32 orbitals) for the π system.
- Setup of a tight-binding Hamiltonian for a zigzag ribbon geometry of width n using the infinite graphene Wannier parameters.
- Substitution of particular on-site and hopping matrix elements ("mix-in") for orbitals close to the ribbon edge (see Fig. 4.9).

The goal is a set of mix-in parameters for the zigzag ribbon edge which generate accurate bands for any ribbon width.

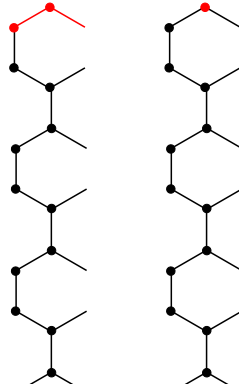


Figure 4.9.: Two different strategies for an edge building block. Left: The building block consists of the two outermost on-site matrix elements (red dots), the 1st-nearest-neighbor hopping matrix element between those two and all hopping matrix elements between those atoms to the adjacent unit cells (red lines). Right: The building block consists of the outermost on-site matrix element and all hopping matrix elements to this atom in the other unit cells.

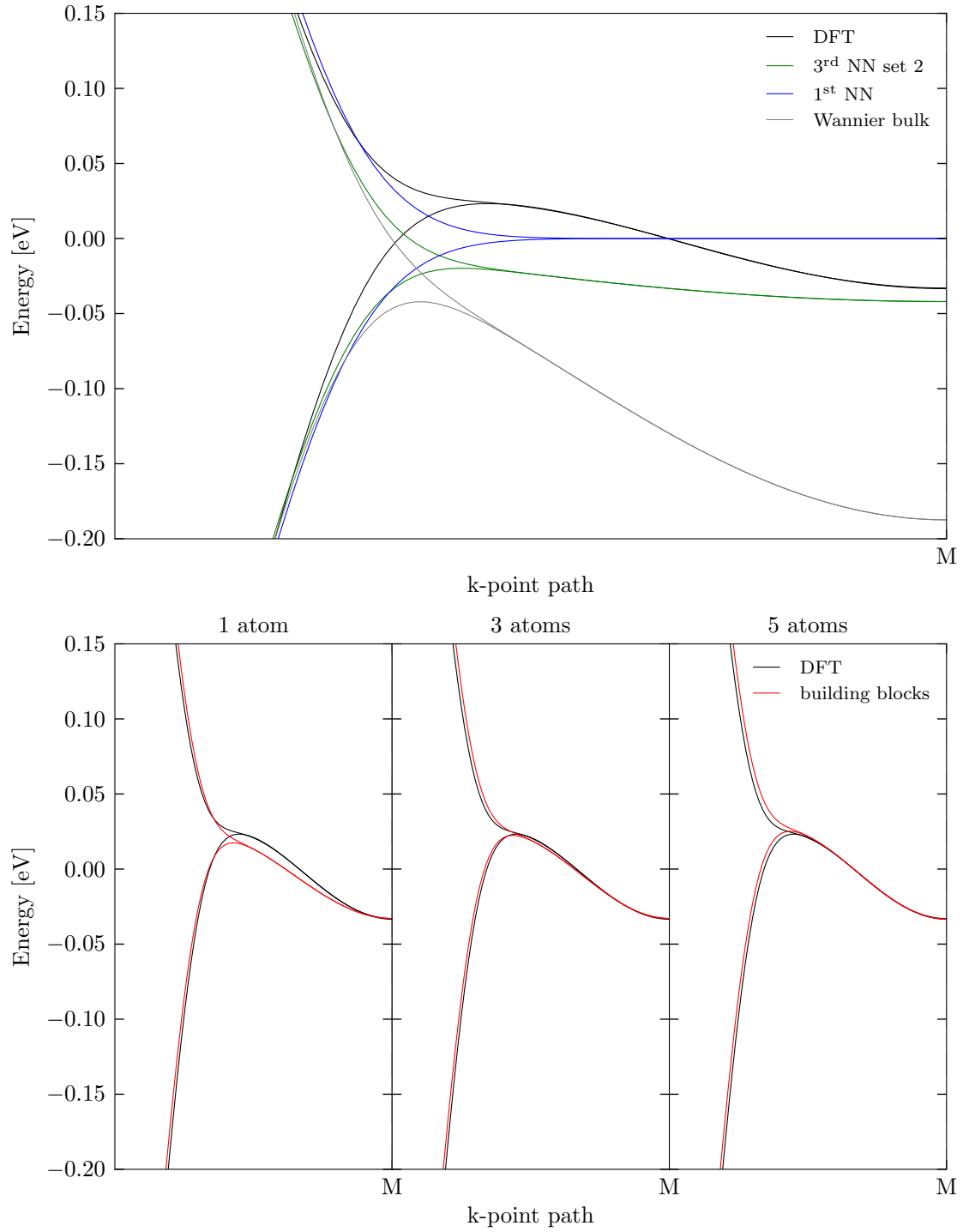


Figure 4.10.: Top: band structure of a 15-zzGNR, calculated using various parameterizations. Bottom: result of the building block system, compared to the DFT band structure. The label "N atoms" refers to a building block consisting of all hopping matrix elements *between* the outermost N atoms of the nanoribbon (including the adjacent unit cells). The band structure created using the building block system (red) changes between the subplots and shows the improvement in quality with a growing number of included atoms.

First, the performance of the mix-in parameters is evaluated for the same ribbon width (15 rings) they were generated with (as a consistency check). The Hamiltonian matrix for this zzGNR-15 is set up, as mentioned, using the Wannier parameters from the bulk graphene calculation, and selected matrix elements are substituted with Wannier parameters from the zzGNR-15 calculation (see Fig. 4.9 for examples).

Fig. 4.10 shows the performance of various selections. A building block, only consisting of the outermost on-site element and the hopping matrix elements between the outermost atoms, already shows a remarkable improvement in comparison to all previous parametrizations. Adding more hopping matrix elements (see figure caption) leads to an better description, but not continuously (e.g. the building block including 4 atoms is better than the building block including 5 atoms).

To demonstrate the application of the building block system, the mix-in parameter set, generated using the zzGNR-15 DFT calculation, is used for a zigzag ribbon with a width of 30 rings. Again, the Hamiltonian matrix is set up using the Wannier bulk parameters, and selected edge parameters are substituted with the mix-in parameters. We use the 1-atom building building block because, though it is less accurate than e.g. the 3-atom building block (see 4.10), it gives a feasible description with a small set of parameters (see Fig. 4.11). The mix-in band does not fit the DFT band as accurately as for the 15-zzGNR. Nevertheless, it is much better than all other parameterizations mentioned in this work.

Most importantly, the edge states (flat part of the π system) are approximately half-occupied (in contrast to the full occupation of the 3rd-nearest-neighbor parameterisation shown in Fig. 4.10). The Fermi energy E_F is at 0 eV – all states below the k axis are occupied, all states above are unoccupied (at $T = 0$).

4.2. Conclusions

Not only can the MLWF procedure create suitable parameters for graphene, but also for much more complicated unit cells containing tens of atoms (Fig. 4.3), which would be impossible using a fitting procedure. The real-space representation of a minimal basis set of a 1-zzGNR can be easily calculated (Fig. 4.4), which show the chemical bonding characteristics of the passivating hydrogen atoms. Using data from nanoribbons up to 30 rings in width, a common behavior of the on-site energies at the edges can be isolated (Figs. 4.6 and 4.7). A combination of MLWF parameters derived from bulk graphene and the edges 15-zzGNR is then used to reproduce the band structure of a 15-zzGNR (Fig. 4.8) and a 30-zzGNR (Fig. 4.11) with much higher accuracy than 3rd-nearest-neighbor tight-binding.

The building block strategy applied here to increase the description quality of the nanoribbon edge can be used to describe adsorbed atoms, missing atoms, Stone-Wales defects etc.

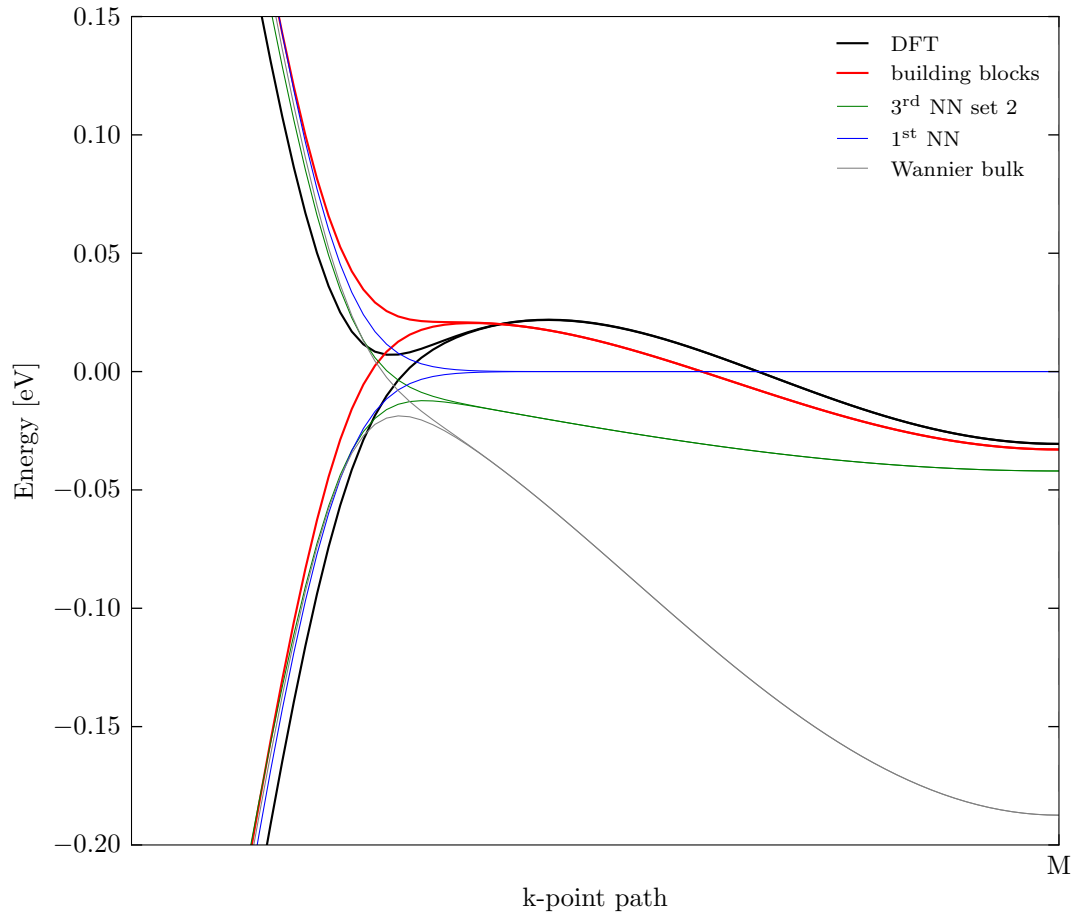


Figure 4.11.: Band structure of a zzGNR-30, calculated using the building block system: DFT (black), 1st-nearest-neighbor (blue), 3rd-nearest-neighbor set 2 (green), building block system (using data from a zzGNR-15 – red), Wannier bulk (gray).

5. Graphene on Ni(111)

The graphene-Nickel interface has interesting spin filtering properties with long coherence times [3, 4, 10, 17, 21]. We want to incorporate those properties into a tight-binding model, including spin, in order to describe realistic interface geometries. In the following, we will show how to create tight-binding parameters for a graphene-Ni(111) slab using the MLWF procedure.

5.1. Model system

The model system consists of six layers of Ni(111) with one layer of graphene on each side. Due to the periodicity of the DFT unit cell in all directions, there is also a z-periodicity so that a layer of vacuum separates an infinite number of "sandwich" structures. This structure was chosen to simulate the behavior of a surface. There is a graphene layer on both sides of the Nickel slab.

Since Nickel is ferromagnetic, one has to consider a spin-dependent band structure. This results in two independent band structures, which are both filled up to a common E_F , leading to a different density of states for each spin. The band structures can each be described by a set of tight-binding parameters, which makes it possible for tight-binding to describe the system including spin.

In the following, spin is not considered, which is the equivalent to looking at one of the two spin channels.



Figure 5.1.: Schematic diagram of the model system.

5.2. Face-centered cubic (fcc) crystal lattice

Bulk Nickel is a face-centered cubic crystal structure with one atom per unit cell.

The basis vectors are:

$$a_1 = \frac{a}{2} \begin{pmatrix} 1 \\ 1 \\ 0 \end{pmatrix}, \quad a_2 = \frac{a}{2} \begin{pmatrix} 0 \\ 1 \\ 1 \end{pmatrix}, \quad a_3 = \frac{a}{2} \begin{pmatrix} 1 \\ 0 \\ 1 \end{pmatrix} \quad (5.1)$$

The band structure $E(k_x, k_y, k_z)$ is usually plotted along the path connecting the points $\Gamma X W L \Gamma K$ (see Fig. 5.2).

The name "face centered cubic" comes from a possible reducible unit cell (see Fig. 5.2) which has Nickel atoms at the eight cube vertices as well as the cube face centers.

The term Ni(111) describes the orientation of the material surface with respect to the crystal structure. The plane which is parallel to the surface has the normal vector $(1, 1, 1)$, written in the basis of the lattice vectors (see above). This is called the *Miller index*.

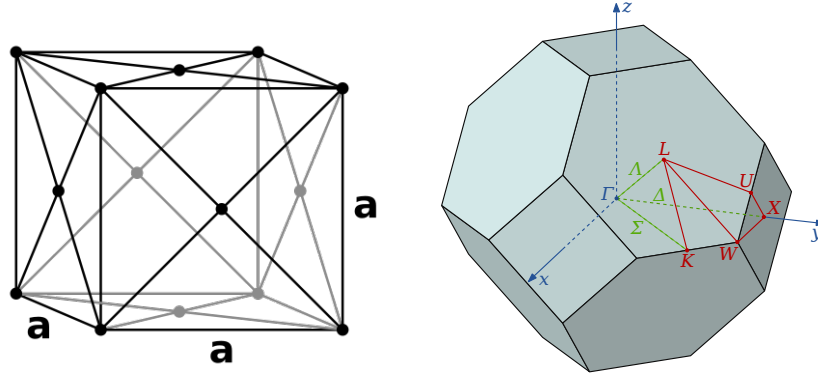


Figure 5.2.: Left: reducible face-centered cubic unit cell [41]. Right: First Brillouin zone of Nickel and symmetry points [42].

5.3. Wannier orbitals of face-centered cubic Nickel

Nickel has 10 valence electrons. As mentioned, a spin-dependent DFT calculation will result in two band structures, one for each spin. The MLWF procedure has to be applied independently to both band structures, identically to a spin-free calculation – but twice. The following procedure is based on a spin-free DFT calculation and is identical to the calculation for one of the spin channels of a spin-dependent calculation.

Fig. 5.7 shows the band structure of a spin-free Nickel fcc calculation. There are hints that d-orbitals will play an important role: First, the majority of the bands are quite flat, which is a property of small, localized orbitals; d-orbitals are more localized than s and p. Secondly, five of the orbitals form groups of three and two degenerate states at the Γ point, which correspond to the e_g - t_{2g} -splitting of d-orbitals.

Additionally, the DFT software may provide projections coefficients of the Bloch states on atomic orbitals as an output, which would also indicate the orbital character.

The d-orbitals are centered on the Nickel atoms. Additional orbitals which describe the chemical bonding and have electron density somewhere between the atoms are necessary. The following guess orbital set is used:

- five d-like orbitals, centered on the Nickel atom
- two s-like orbitals, centered at $\frac{1}{4}(1, 1, 1)$ and $\frac{3}{4}(1, 1, 1)$ (in lattice coordinates)

Those are initial guess orbitals: e.g. the converged versions of the initially guessed s-orbitals may not be spherically symmetric. Most of the electron density, though, is already in the right place. The upper boundaries of the outer and frozen energy window are 40 and 14 eV.

Fig. 5.5 shows the result of this calculation. The bands below and around E_F are described perfectly; in the region up to 10 eV above E_F discrepancies occur. More orbitals would be needed in order to describe this region and the higher bands. To explore the behavior for a varying number of Wannier orbitals, a version with five orbitals (only the d-orbitals as a starting guess) was calculated (Fig. 5.5). Parts of the flat bands around E_F are described well; the bands going down and up and the Γ point are not described at all. Most importantly, some bands near E_F are described very badly, what makes this parameterization unsuitable for conductance calculations.

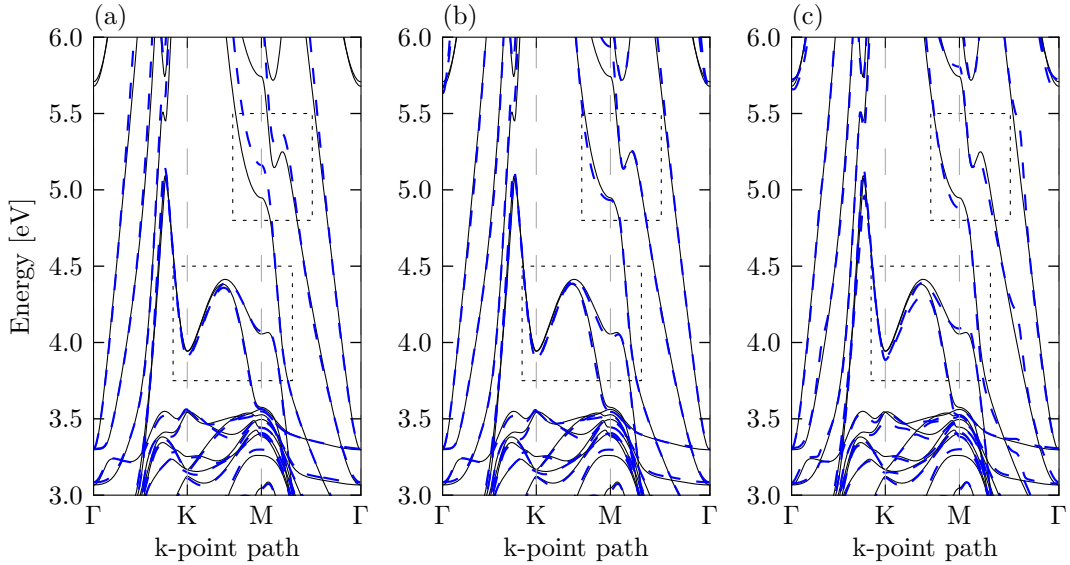


Figure 5.3.: DFT (black) and Wannier (blue) band structure of the graphene on a Ni(111) slab with different upper boundaries of the frozen energy window (a) 5 eV (b) 6 eV (c) 7 eV. The dashed rectangles mark regions of the band structure with strongly change with the chosen upper boundary.

5.4. Wannier orbitals of graphene on Ni(111)

Putting together the information gained from the analysis of bulk fcc Nickel and graphene, the initial guess orbitals for the combined slab were chosen the same as for the separate materials. As depicted in Fig. 5.5, some features from fcc-Nickel and graphene are still visible: the flat d-bands of Ni around E_F as well as the σ system of graphene. The graphene Dirac cone, however, is not visible any more due to coupling of the p_z orbitals to the Nickel slab.

The accuracy of the bands below E_F is high, while the reproduction of the higher bands is delicate. Their quality strongly depends on the upper border of the outer energy window, especially the bands between 5 and 8 eV. The upper boundary of the outer window is 25 eV to include the complete set of bands that occur in the Fermi energy region. The upper boundary of the frozen window was varied between 5 and 7 eV (see Fig. 5.3), and 6 eV was finally chosen as the best value.

In this parameterization, the Wannier orbitals describe the system well up to approx. 5.5 eV (2 eV above E_F). Fig. 5.8 shows the real-space representation of the resulting basis orbitals. In Fig. 5.6, the Wannier band structure is depicted for various cutoff configurations. The quality of the description increases with the number of included hopping parameters.

#	type	x	y	z	spread
1-3	e_g	0	0	0	0.4069
4-5	t_{2g}	0	0	0	0.4518
6	s	0.855	0.855	0.855	1.604
7	s	2.565	0.565	0.565	1.604

Figure 5.4.: Centers and spreads of the Wannier orbitals in real-space representation.

5.5. Conclusions

Fcc-Nickel can be described using 7 MLWFs accurately up to about 10 eV above the Fermi level (Fig. 5.7). These orbitals can be used as a starting guess for a Graphene-Ni-interface. The resulting MLWF band structure (Fig. 5.5) reproduces the complex DFT band structure very well below and around the Fermi energy. The quality of the bands above the Fermi energy strongly depends on the choice of the upper border of the frozen energy window (Fig 5.3). The qualitatively accurate parameterization of the material interface provides a tool to perform tight-binding transport calculations without further approximations. A additional increase of the thickness of the Ni part could make a separation of the Ni bulk and graphene-Ni-surface conductance behavior possible.

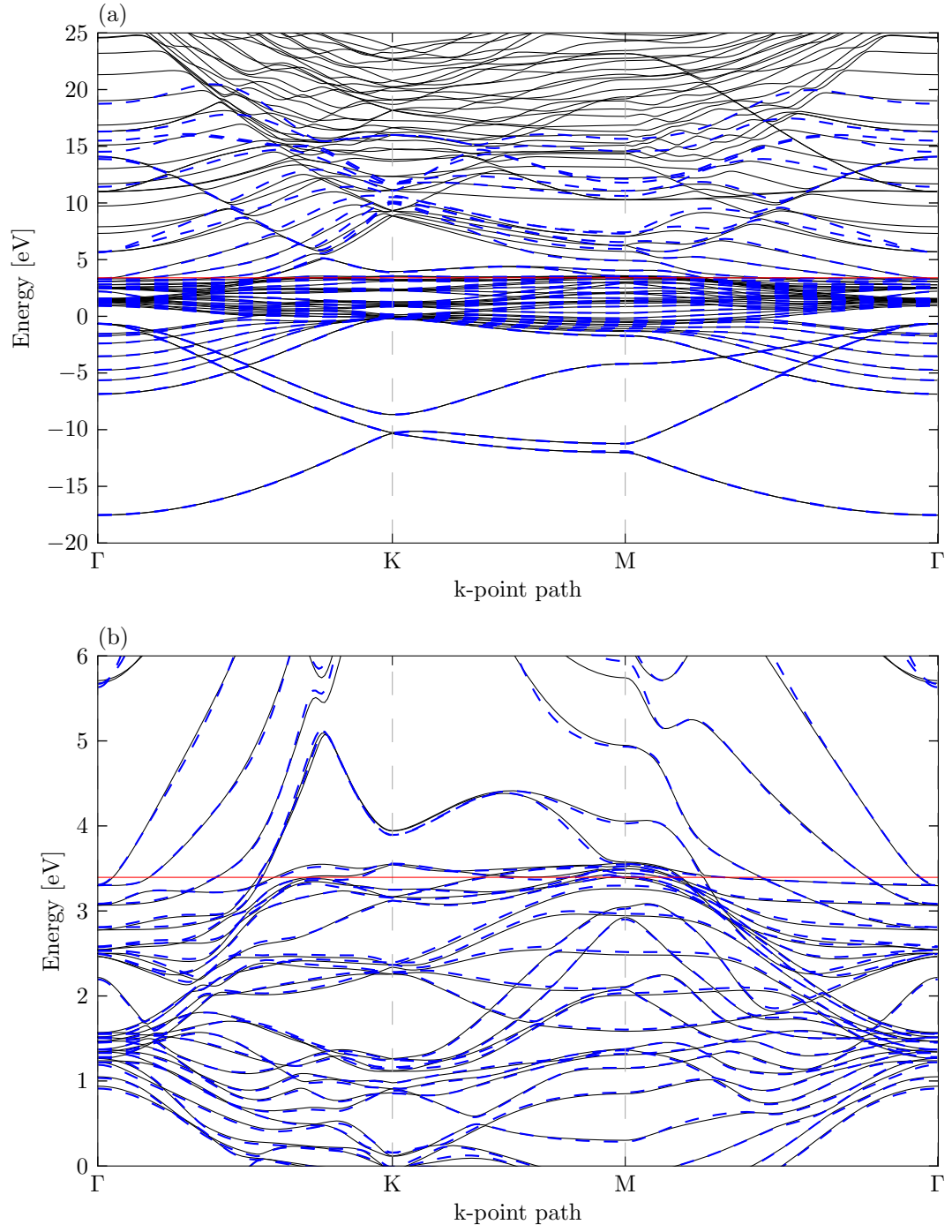


Figure 5.5.: Band structure of the graphene on a Ni(111) slab: DFT (black) and MLWF (blue). (b) shows an enlargement of (a) near E_F (red line).

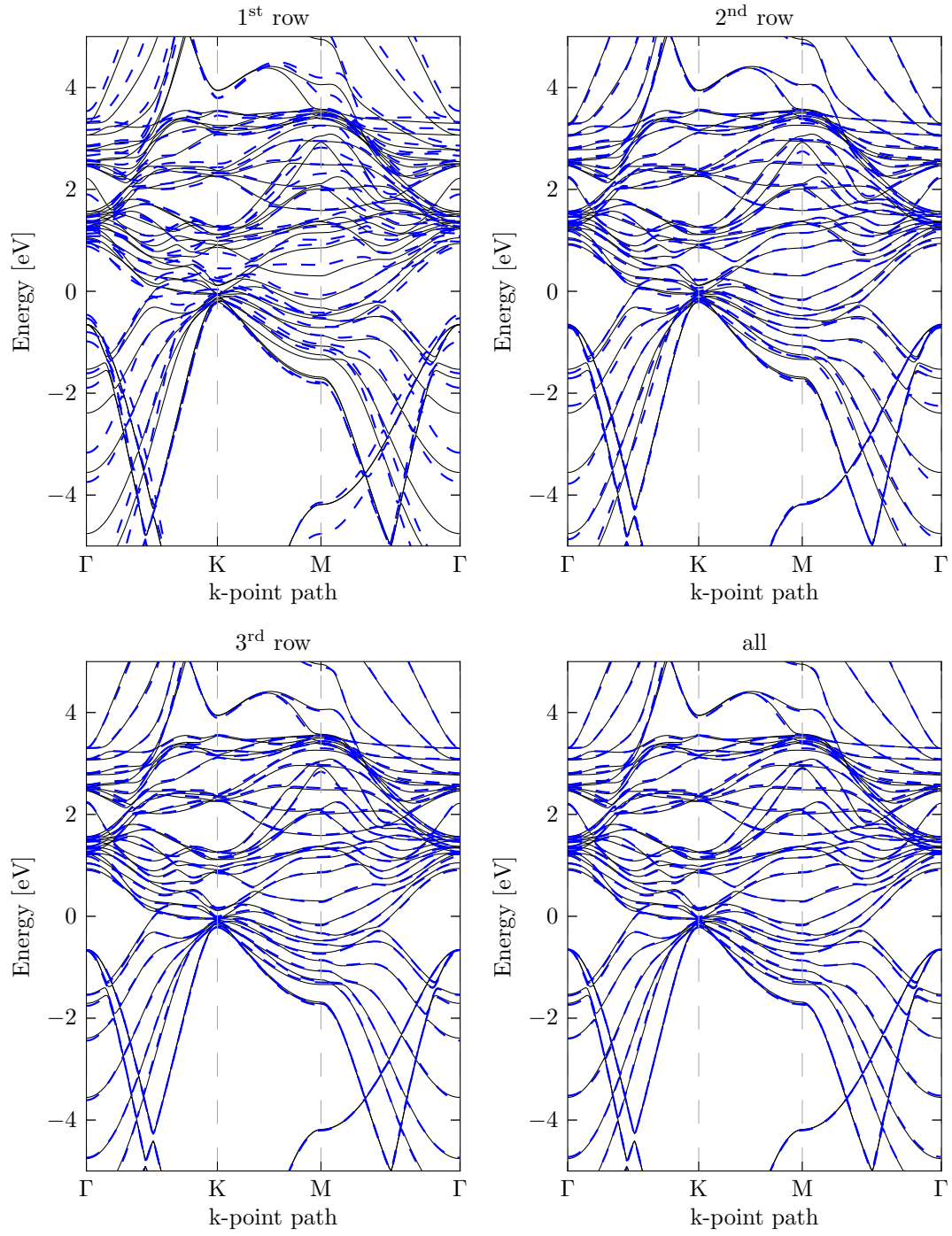


Figure 5.6.: Band structure of the graphene on Ni(111) slab: DFT (black) and Wannier (blue). The number of used hopping parameters is varied. The row number refers to the number of neighbor cell rows that surround the main cell.

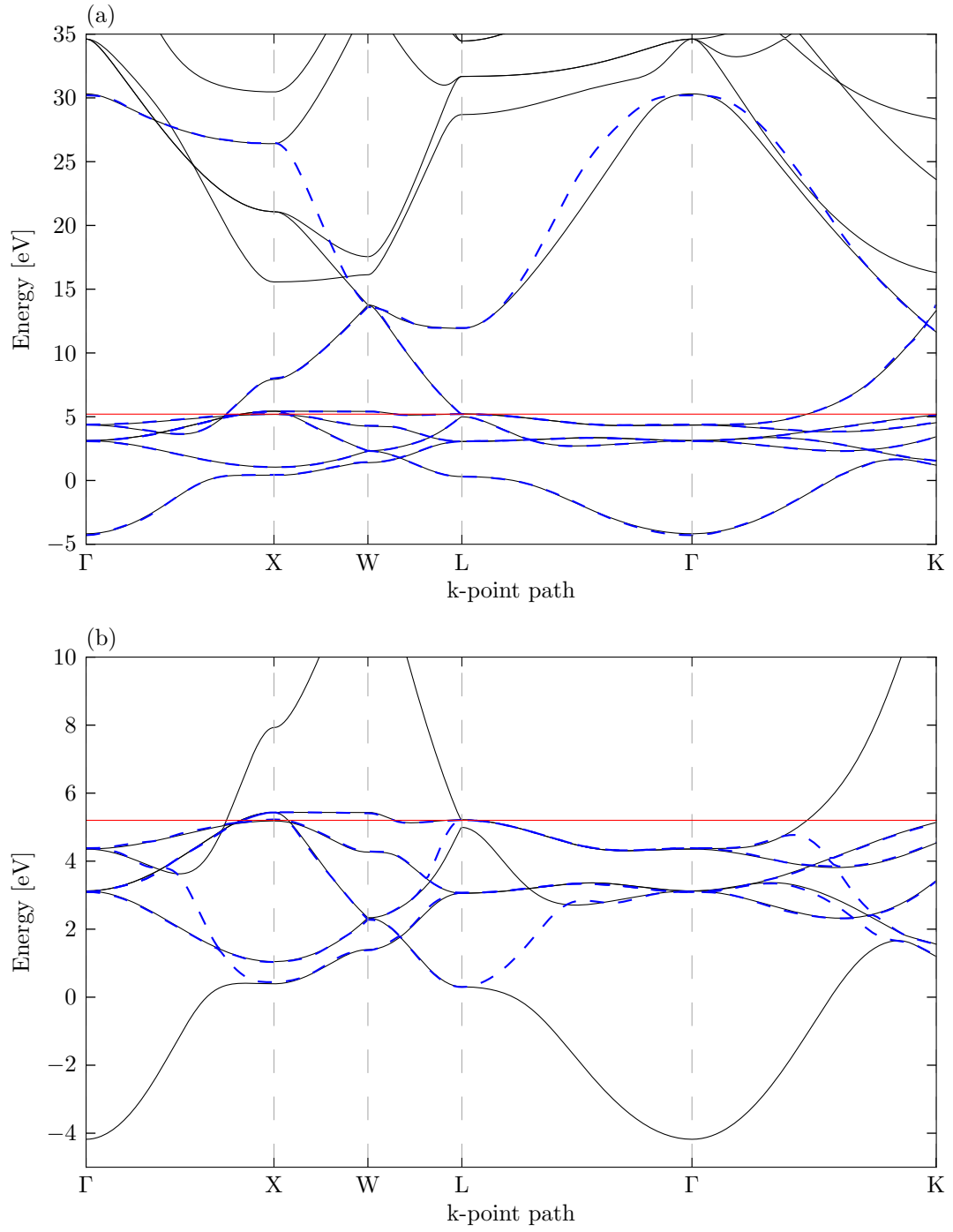


Figure 5.7.: Band structure of Nickel fcc. (a) DFT (black) and MLWF with 7 orbitals (blue) (b) DFT (black) and MLWF with 5 orbitals (blue). The red line marks E_F .

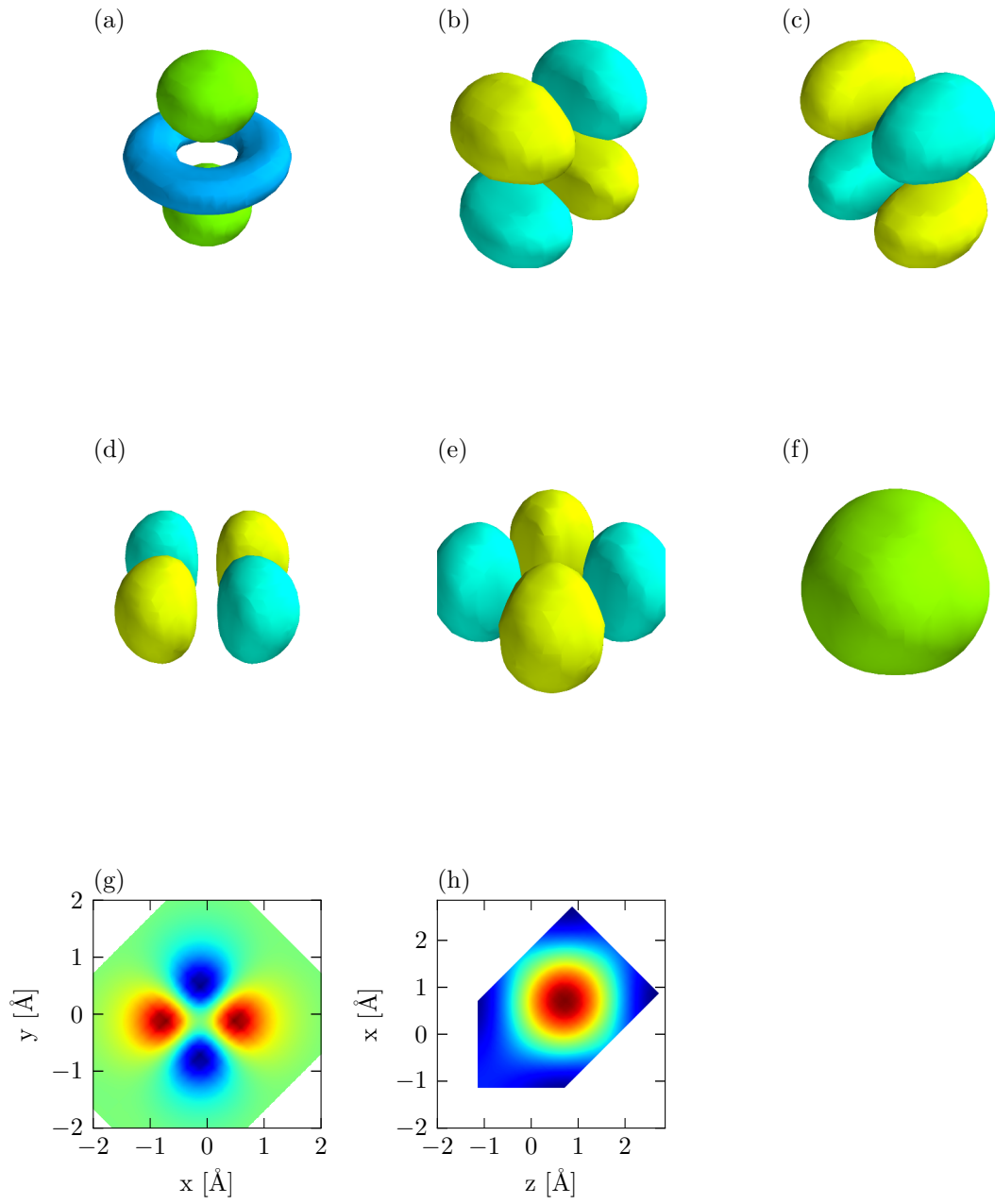


Figure 5.8.: Plots of the MLWFs for Ni-fcc. (a)-(e) the five d-like orbitals, centered on the Nickel atom (f) the s-like orbital (g) a cut through the donut-like d-orbital (h) a cut through the s-like orbital.

6. Polycyclic aromatic hydrocarbons

PAHs are the "microscopic" counterpart of graphene in chemistry. While high-level quantum chemistry is not yet able to calculate structures of the size of graphene flakes, we try to see trends in the results for small molecules with a size of less than 20 rings that we can transfer to bigger systems. One of those trends is the chemical radicality. In terms of a single Slater determinant, a singly occupied molecular orbital leads to a higher reactivity of the molecule. For high-level quantum chemistry calculations, a similar tool is the natural orbital occupation. If there are natural orbitals with an occupation significantly different from 2 or 0, the system tends to be radical, and it is also a sign for strong correlation effects.

Natural orbitals are one way to go from the results of high-level quantum chemistry calculations to a set of single-particle orbitals with occupation numbers. This should provide a bridge to tight-binding where single-particle orbitals are an absolute necessity. Since single-particle energies are also required for constructing a tight-binding Hamiltonian, we investigate the Hartree-Fock energies of the natural orbitals, including a disentanglement procedure to avoid fractional occupations.

Instead of working towards an accurate value of total energy, we look into the description of the valence system, where correlation has its biggest influence, and try to capture those effects by applying a Hartree-Fock operator on the natural orbitals.

In the following, the procedure will be illustrated for naphthalene using previously calculated natural orbitals [28].

6.1. Comparison of quantum chemistry methods and tight-binding

Tight-binding uses results from other approximation methods, specifically single-particle wave functions and energies. Both density-functional theory and the Hartree-Fock method produce them. There are other methods based on Hartree-Fock (most of them called Post-Hartree-Fock methods) which are more accurate but do not supply information about single-particle states.

Tight-binding parameters can be created from a set of single-particle wave functions (i.e. molecular orbitals) $|\varphi_i\rangle$ and their single-particle energies ε_i . The single-particle Hamiltonian H_{SP} in the basis $|\varphi_i\rangle$ is

$$H_{ij} = \langle \varphi_i | H_{\text{SP}} | \varphi_j \rangle = \begin{pmatrix} \varepsilon_1 & & & \\ & \varepsilon_2 & & \\ & & \varepsilon_3 & \\ & & & \varepsilon_4 \\ & & & & \ddots \end{pmatrix} = \delta_{ij} \varepsilon_i \quad (6.1)$$

A tight-binding Hamiltonian can be found by a transformation to a localized basis set $|\phi_i\rangle$:

$$\tilde{H}_{ij} = \langle \phi_i | H_{\text{SP}} | \phi_j \rangle = \sum_{k,l} \langle \phi_i | \varphi_k \rangle \langle \varphi_k | H_{\text{SP}} | \varphi_l \rangle \langle \varphi_l | \phi_j \rangle = \mathbf{U} \mathbf{H} \mathbf{U}^{-1} \quad (6.2)$$

The matrix elements in \tilde{H}_{ij} are tight-binding parameters. This is essentially the same transformation as in the MLWF procedure; Wannier functions are one possible choice of localized basis functions $|\phi_i\rangle$. The basis set does not have to be complete, but should describe the molecular orbitals $|\varphi_i\rangle$ as well as possible.

This shows that a set of molecular orbitals $(|\varphi_i\rangle, \varepsilon_i)$ is the basic ingredient of a tight-binding description.

Hartree-Fock solves the Schrödinger equation using a single Slater determinant, built from molecular orbitals, as an ansatz [9, p. 87]:

$$\Psi(\mathbf{r}_1, \mathbf{r}_2, \dots, \mathbf{r}_N) = \frac{1}{\sqrt{N!}} \begin{vmatrix} \varphi_1(\mathbf{r}_1) & \varphi_2(\mathbf{r}_1) & \cdots & \varphi_N(\mathbf{r}_1) \\ \varphi_1(\mathbf{r}_2) & \varphi_2(\mathbf{r}_2) & \cdots & \varphi_N(\mathbf{r}_2) \\ \vdots & \vdots & \ddots & \vdots \\ \varphi_1(\mathbf{r}_N) & \varphi_2(\mathbf{r}_N) & \cdots & \varphi_N(\mathbf{r}_N) \end{vmatrix}, \quad (6.3)$$

where N is the number of electrons and $|\varphi_i\rangle$ are molecular orbitals. The ground state of the system is the wave function $|\Psi\rangle$ that minimizes the energy functional

$$E = \frac{\langle \Psi | H | \Psi \rangle}{\langle \Psi | \Psi \rangle}, \quad (6.4)$$

leading to a system of coupled eigenvalue problems [9, pp. 86-92]

$$F|\varphi_i\rangle = \varepsilon_i|\varphi_i\rangle, \quad (6.5)$$

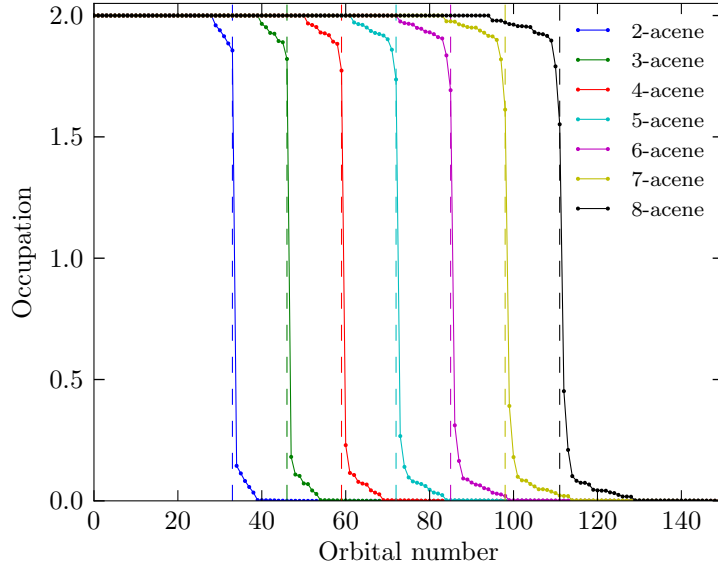


Figure 6.1.: Natural orbital occupations for n -acenes for $n = 2 - 8$ [28]. With increasing molecule size, the number of occupied electronic orbitals grows. For each molecule, the orbitals are sorted by occupation number. All orbitals with a fractional occupation belong to the π or π^* system. The highest orbital with an occupation number greater than 1 (marked by dashed lines) corresponds to the Fermi level of a single-particle theory.

where F is the Fock operator, an effective one-electron energy operator. It assigns an energy to each molecular orbital $|\varphi_i\rangle$. The resulting molecular orbitals $|\varphi_i\rangle$ with energies ε_i describe molecular wave functions of single electrons and fulfill all requirements for a transformation to tight-binding parameters. The number of orbitals might be greater than the number of electrons, depending on the size of the basis set used in the Hartree-Fock calculation. In that case, a subset of the orbitals is selected in order to minimize the total energy; they are sorted by their energy ε_i , and the first N orbitals are occupied with one electron each (their occupation number η_i is one), and all other orbitals with higher energies, the virtual orbitals, are occupied with zero electrons each (η_i is zero). The density is thus

$$\varrho(\mathbf{r}) = \sum_i \eta_i \varphi_i^*(\mathbf{r}) \varphi_i(\mathbf{r}). \quad (6.6)$$

Regarding the allowed occupation numbers, there are two methods: restricted Hartree-Fock (RHF) and unrestricted Hartree-Fock (UHF, [9, pp. 120-121] and [40, pp. 206ff.]). RHF only allows occupation numbers of 2 (spin degeneracy) and 0, whereas UHF also allows occupation 1, and α and β spin electrons do not necessarily have the same real-space molecular wave functions $\varphi_i(\mathbf{r})$.

Post-Hartree-Fock and related methods do not result in single-particle energies. Instead of a single Slater determinant, the ansatz is a linear combination of Slater determinants

$|\Phi_i\rangle$ [9, pp. 154ff.]:

$$|\Psi\rangle = \sum_i A_i |\Phi_i\rangle. \quad (6.7)$$

Each $|\Phi_i\rangle$ is a determinant analogous to $|\Psi\rangle$ in Eq. 6.3, but with a unique set of orbitals $|\varphi_i\rangle$. One of the possible methods in Post-Hartree-Fock calculations is to perform a Hartree-Fock calculation of a molecule and build the determinants $|\Phi_i\rangle$ from different subsets of the Hartree-Fock molecular orbitals (occupied and virtual) with a subsequent variation of the coefficients A_i to find the ground state wave function $|\Psi\rangle$.

$|\Psi\rangle$ is called a correlated wave function. Electrons no longer occupy a fixed molecular orbital with a fixed energy. The probability to find the system in the state $|\Phi_i\rangle$ is $|\langle\Phi_i|\Psi\rangle|^2 = A_i^2$. In every determinant of the expansion (Eq. 6.7), the electrons may occupy different molecular orbitals.

There are several methods [9] which mainly differ in the combination of molecular orbitals that in each determinant and which orbitals are varied in the minimization of the energy functional. In any case, there is no direct way to assign molecular orbitals and energies to the electrons. In the following, we are looking for an approximate solution to this problem.

Quantum chemistry and tight-binding have at least one link: the ground state with its density $\varrho(\mathbf{r})$ and energy E . We try to extract information from $\varrho(\mathbf{r})$ that we can use to create tight-binding parameters; specifically, with the help of so-called natural orbitals.

Natural orbitals φ_i are the orbitals that diagonalize the one-particle density matrix. The transformation to the real-space one-particle density matrix $\varrho(\mathbf{r}, \mathbf{r}')$ is

$$\varrho(\mathbf{r}, \mathbf{r}') = \sum_i \eta_i \varphi_i^*(\mathbf{r}) \varphi_i(\mathbf{r}'), \quad (6.8)$$

where η_i is the eigenvalue corresponding to the eigenstate φ_i . Fig. 6.1 shows natural orbital occupations for n-acenes.

Natural orbitals are an orthogonal basis that can reproduce the ground state density. Due to the similarity of Eq. 6.8 to Eq. 6.6 they can be interpreted as molecular orbitals of a single-particle calculation, but with possibly non-integer occupation numbers η_i . If there was a way to assign energies ε_i , we could create a tight-binding parameterization with a ground state that is identical to the one of the quantum chemistry calculation.

We will calculate such energies ε_i using the single-particle Hamiltonian (H_{SP} in Eq. 6.1) of the Hartree-Fock approximation: the Fock operator F (Eq. 6.5), describing the kinetic energy of an electron and the attraction to all the nuclei, as well as the repulsion to all the other electrons ([9, p. 91] and [40, pp. 114ff.]). F contains all molecular orbitals of the determinant φ_i as well as the occupation numbers η_i , which is the reason why the Hartree-Fock method is also called Self-Consistent Field method.

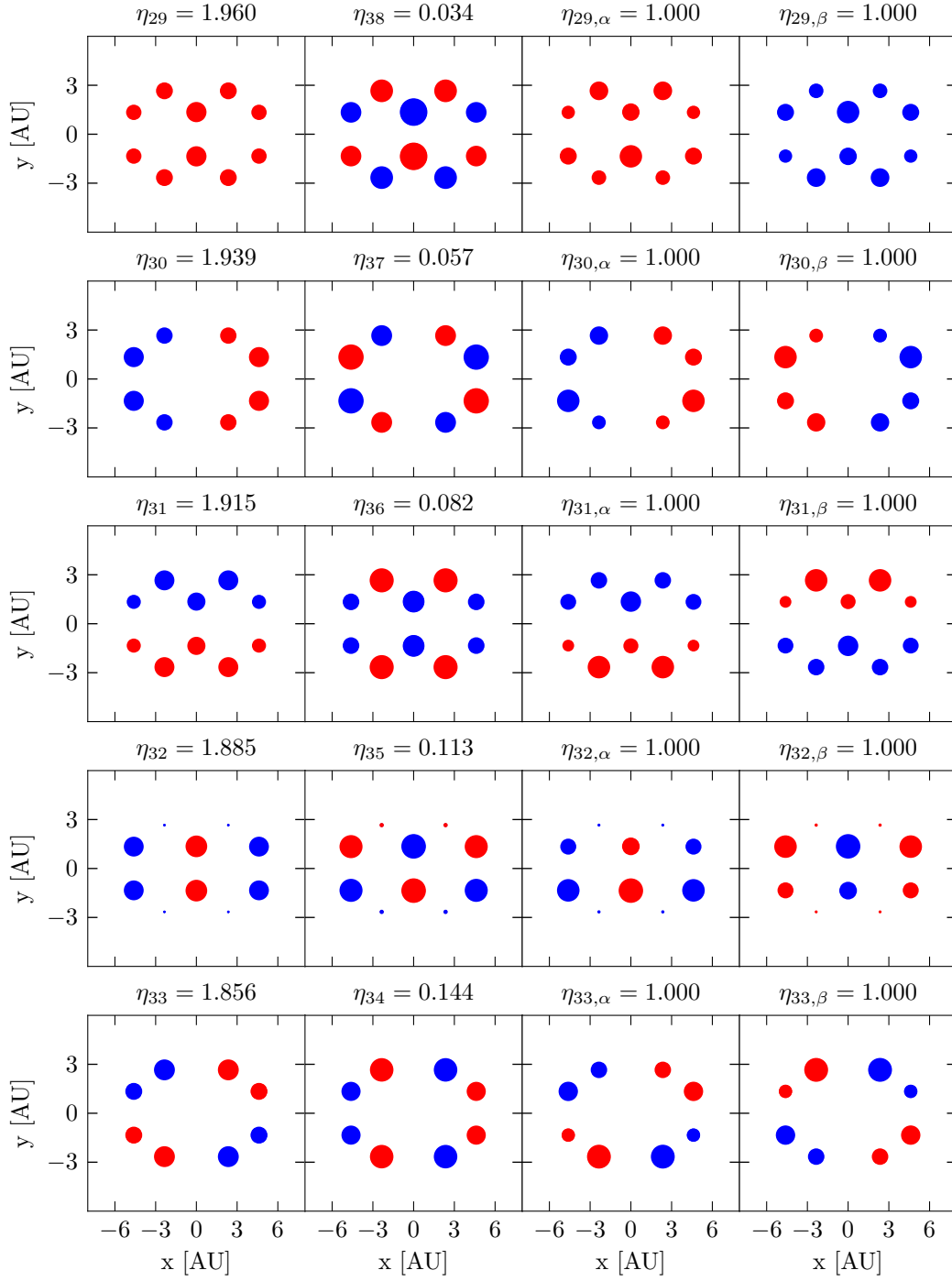


Figure 6.2.: Natural orbitals of the π system of naphthalene (2-acene) with fractional occupation (left columns – compare to the curve in Fig. 6.1), and the occupied disentangled orbitals ($\eta = 1$). The radii are proportional to the orbital amplitudes. Note the symmetry relation between the original orbitals (left) and the slightly less symmetric disentangled orbitals (right).

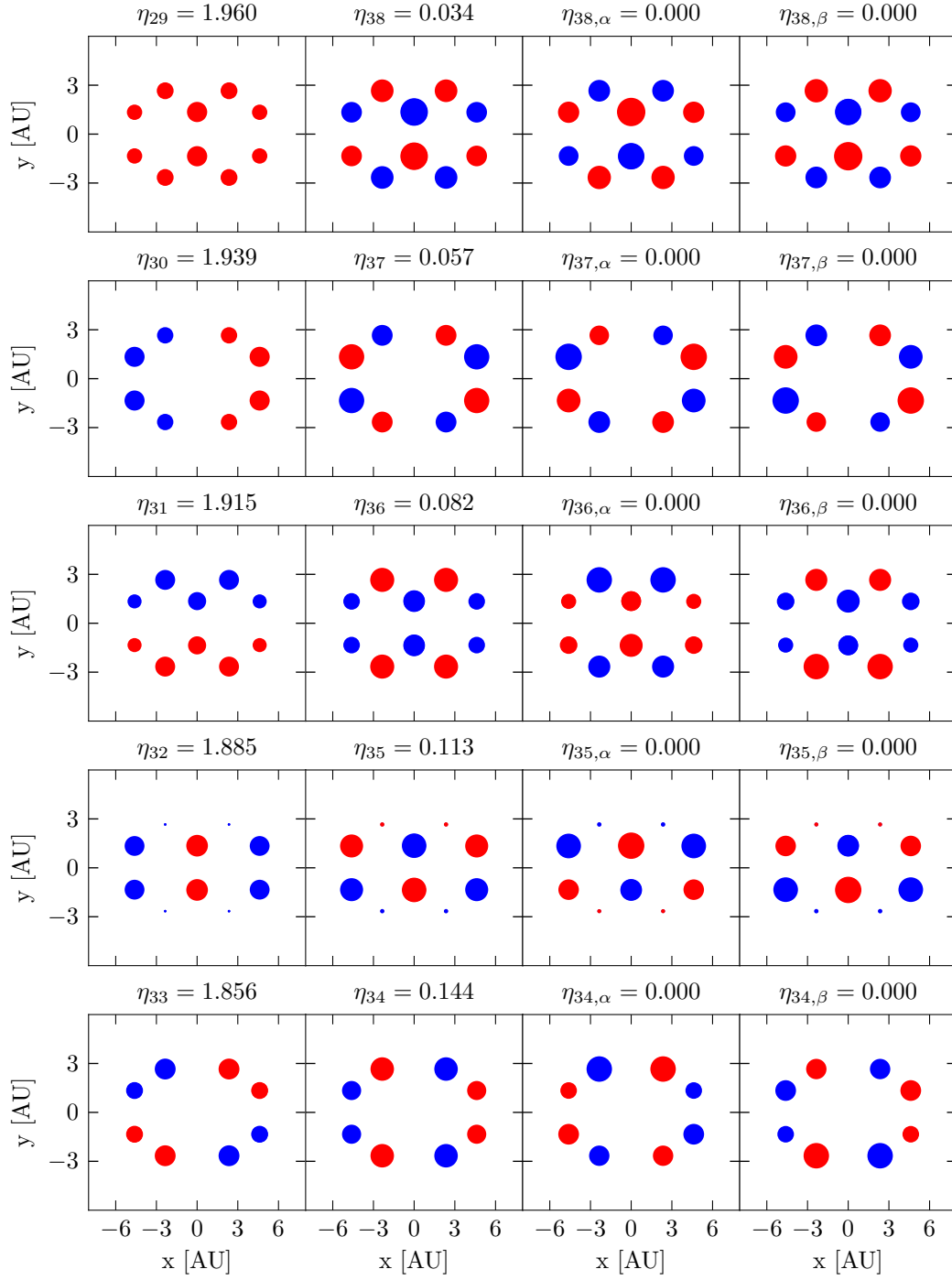


Figure 6.3.: Natural orbitals of the π system of naphthalene with fractional occupation (left columns), and the virtual disentangled orbitals ($\eta = 0$).

6.2. Disentangling fractionally occupied natural orbitals

As an intermediate step, the natural orbitals have to be modified to accomodate the inability of the Fock operator to handle occupation numbers η_i other than 0 and 2 (RHF) or 0, 1 and 2 (UHF). All natural orbitals with a fractional occupation are transformed using a so-called disentanglement transformation [1] (note that the term "disentanglement" is used in a different context than in the other chapters of this work). After this unitary transformation to spin orbitals (UHF), all previously fractionally occupied orbitals have occupation 1 or 0, while the total electron density is conserved.

Note that the doubly occupied natural orbitals do not contain useful information about single electron states because they span a degenerate eigenspace of the density matrix and are therefore not unique. The same statement is valid for the unoccupied orbitals.

The electron density for a set of natural orbitals φ_i with occupation numbers η_i is

$$\rho(\mathbf{r}) = \sum_i \eta_i \varphi_i^*(\mathbf{r}) \varphi_i(\mathbf{r}) \quad (6.9)$$

Let the range of the orbitals participating in the transformation (the fractionally occupied ones, that is) be given by n_{\min} and n_{\max} . Then, for a pair of orbitals φ_a and φ_b from this range, the transformation is

$$\begin{pmatrix} \tilde{\varphi}_{a,\alpha}(\mathbf{r}) \\ \tilde{\varphi}_{a,\beta}(\mathbf{r}) \\ \tilde{\varphi}_{b,\alpha}(\mathbf{r}) \\ \tilde{\varphi}_{b,\beta}(\mathbf{r}) \end{pmatrix} = \begin{pmatrix} \sqrt{\frac{\eta_a}{2}} & 0 & \sqrt{\frac{\eta_b}{2}} & 0 \\ 0 & -\sqrt{\frac{\eta_a}{2}} & 0 & \sqrt{\frac{\eta_b}{2}} \\ \sqrt{\frac{\eta_b}{2}} & 0 & -\sqrt{\frac{\eta_a}{2}} & 0 \\ 0 & \sqrt{\frac{\eta_b}{2}} & 0 & \sqrt{\frac{\eta_a}{2}} \end{pmatrix} \begin{pmatrix} \varphi_a(\mathbf{r}) \\ \varphi_a(\mathbf{r}) \\ \varphi_b(\mathbf{r}) \\ \varphi_b(\mathbf{r}) \end{pmatrix} \quad (6.10)$$

with occupations $\eta_{a,\alpha} = \eta_{a,\beta} = 1$ and $\eta_{b,\alpha} = \eta_{b,\beta} = 0$. The transformed orbitals with integer occupations create the same electron density as the original with their fractional occupations η_a and η_b . They are assigned different spin, α and β , respectively, which preserves their orthogonality. In the above notation, the original natural orbitals are also interpreted as carriers of two electrons of opposite spin, leading to four instead of two original orbitals.

The transformation in Eq. 6.10 is unitary if $\eta_a + \eta_b = 2$ (proof e.g. by calculating the eigenvalues of the two 2×2 subblocks). This is (approximately) the case if a and b are symmetric w.r.t. the orbital window (see Fig. 6.1 – also Fig. 6.2 for symmetry relations); expressed mathematically, this is $b = n_{\max} - (a - n_{\min})$. Since the aforementioned sum is not exactly 2, the unitarity is slightly breached.

The density $\rho_{a,b}$ associated with φ_a and φ_b can be written in terms of the new, disentangled orbitals:

$$\varphi_a(\mathbf{r}) = \sqrt{\frac{1}{2\eta_a}} \tilde{\varphi}_{a,\alpha}(\mathbf{r}) - \sqrt{\frac{1}{2\eta_a}} \tilde{\varphi}_{a,\beta}(\mathbf{r}) \quad (6.11)$$

$$\varphi_b(\mathbf{r}) = \sqrt{\frac{1}{2\eta_b}} \tilde{\varphi}_{a,\alpha}(\mathbf{r}) + \sqrt{\frac{1}{2\eta_b}} \tilde{\varphi}_{a,\beta}(\mathbf{r}) \quad (6.12)$$

By expressing the total density contribution $\varrho_{a,b}$ from the orbitals $\varphi_a(\mathbf{r})$ and $\varphi_b(\mathbf{r})$, we can show that the density is preserved, but with integer occupations:

$$\varrho_{a,b} = \eta_a \varphi_a^2 + \eta_b \varphi_b^2 \quad (6.13)$$

$$= \eta_a \left(\sqrt{\frac{1}{2\eta_a}} \tilde{\varphi}_{a,\alpha} - \sqrt{\frac{1}{2\eta_a}} \tilde{\varphi}_{a,\beta} \right)^2 + \eta_b \left(\sqrt{\frac{1}{2\eta_b}} \tilde{\varphi}_{a,\alpha} + \sqrt{\frac{1}{2\eta_b}} \tilde{\varphi}_{a,\beta} \right)^2 \quad (6.14)$$

$$= \eta_a \frac{1}{2\eta_a} (\tilde{\varphi}_{a,\alpha} - \tilde{\varphi}_{a,\beta})^2 + \eta_b \frac{1}{2\eta_b} (\tilde{\varphi}_{a,\alpha} + \tilde{\varphi}_{a,\beta})^2 = \quad (6.15)$$

$$= \frac{1}{2} \left[(\tilde{\varphi}_{a,\alpha} - \tilde{\varphi}_{a,\beta})^2 + (\tilde{\varphi}_{a,\alpha} + \tilde{\varphi}_{a,\beta})^2 \right] \quad (6.16)$$

$$= 1 \tilde{\varphi}_{a,\alpha}^2 + 1 \tilde{\varphi}_{a,\beta}^2 = \eta_{a,\alpha} \tilde{\varphi}_{a,\alpha}^2 + \eta_{a,\beta} \tilde{\varphi}_{a,\beta}^2 \quad (6.17)$$

6.3. Hartree-Fock expectation values

Having arrived at singly occupied (instead of fractionally) and unoccupied natural orbitals (right two columns of Figs. 6.2 and 6.3), we calculate their expectation value of the unrestricted Hartree-Fock operator $\varepsilon_i = \langle \tilde{\varphi}_{i,\alpha} | F | \tilde{\varphi}_{i,\alpha} \rangle = \langle \tilde{\varphi}_{i,\beta} | F | \tilde{\varphi}_{i,\beta} \rangle$.

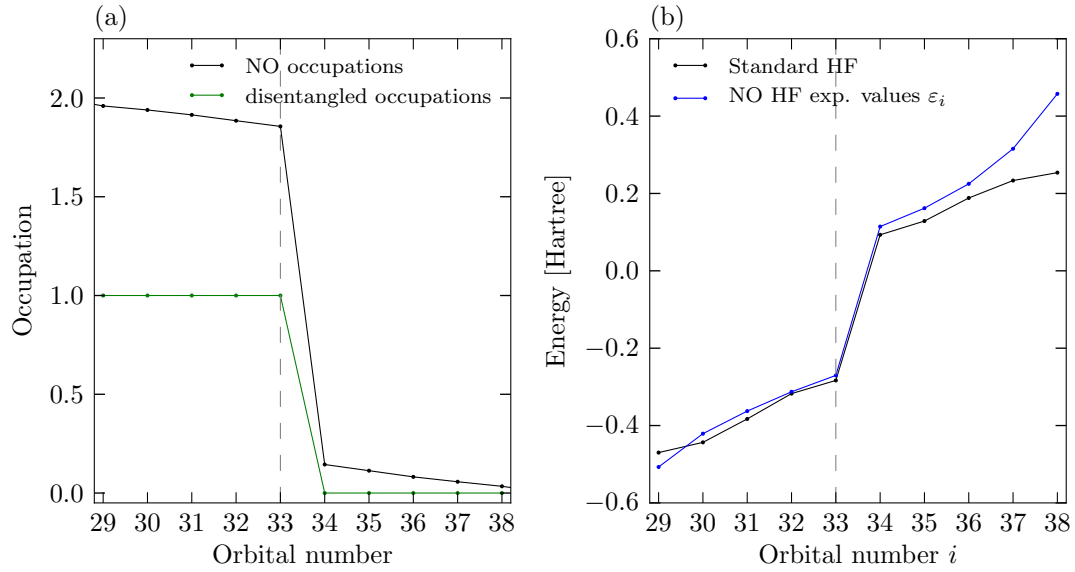


Figure 6.4.: (a) π orbital occupations of naphthalene before and after the disentanglement procedure (b) π orbital energies of naphthalene: standard Hartree-Fock calculation (black), Hartree-Fock expectation values of the disentangled NOs (ordered by orbital number n , see Figs. 6.2 and 6.3). The dashed gray line marks the last fully occupied orbital (according to the NO occupations).

The result is shown in Fig. 6.4, together with the orbital energies of a standard UHF calculation for comparison.

The expectation values are identical for α and β spin because $|\tilde{\varphi}_{i,\alpha}\rangle = -S_0|\tilde{\varphi}_{i,\beta}\rangle$, where S_0 is the reflection across the x axis, and the Fock operator is invariant under this transformation ($F = S_0 F S_0^T$).

Nearly all NO energy expectation values are slightly greater than their HF pendants.

First, the total energy of a determinant built from NOs is higher than the total energy of the result of a HF calculation, simply because the latter is the result of a minimization of the total energy of a single determinant. Since the relative deviation of the NOs from the HF molecular orbitals is small, it is plausible that the expectation values will slightly differ from the orbital energies and will have a tendency to be greater.

Second, the disentangled NOs are less symmetric than the original NOs and the Hartree-Fock orbitals and have higher density variations, which leads to a greater kinetic energy contribution to the energy expectation value. The potential energy and the exchange energy change in a less obvious manner because all NOs contribute to the respective terms in the Fock operator.

The disentangled orbitals and the Hartree-Fock expectation values together form the set of single-particle orbitals and energies that can be transformed to tight-binding matrix elements.

6.4. Conclusions

We transformed (Eq. 6.10) natural orbitals describing naphthalene from a quantum chemistry calculation to orbitals with integer occupation that create the same electron density. We assigned them energies using an unrestricted Hartree-Fock operator (Fig. 6.2), with the intention of using the orbitals and energies for tight-binding calculations, analogous to DFT Kohn-Sham orbitals and their energies.

To create useful building blocks, as described in the previous chapters, more PAHs of varying sizes need to be analysed, with the goal of finding reusable patterns in the on-site energies and hopping parameters.

A. Appendix

A.1. Software

The calculations were done on workstations and on the Vienna Scientific Cluster (VSC-2).

Third-party physics software

- DFT calculations: VASP 5.2.12
- MLWF procedure: wannier90 1.2
- Hartree-Fock calculations: MOLCAS 7.6

Third-party general software and modules

- Development environment: Ubuntu, Mathematica, IPython, Python
- Parallelization: Open MPI
- Visualization: Matplotlib, Mayavi2, Inkscape
- Numerical libraries: Numpy, Scipy, Intel MKL

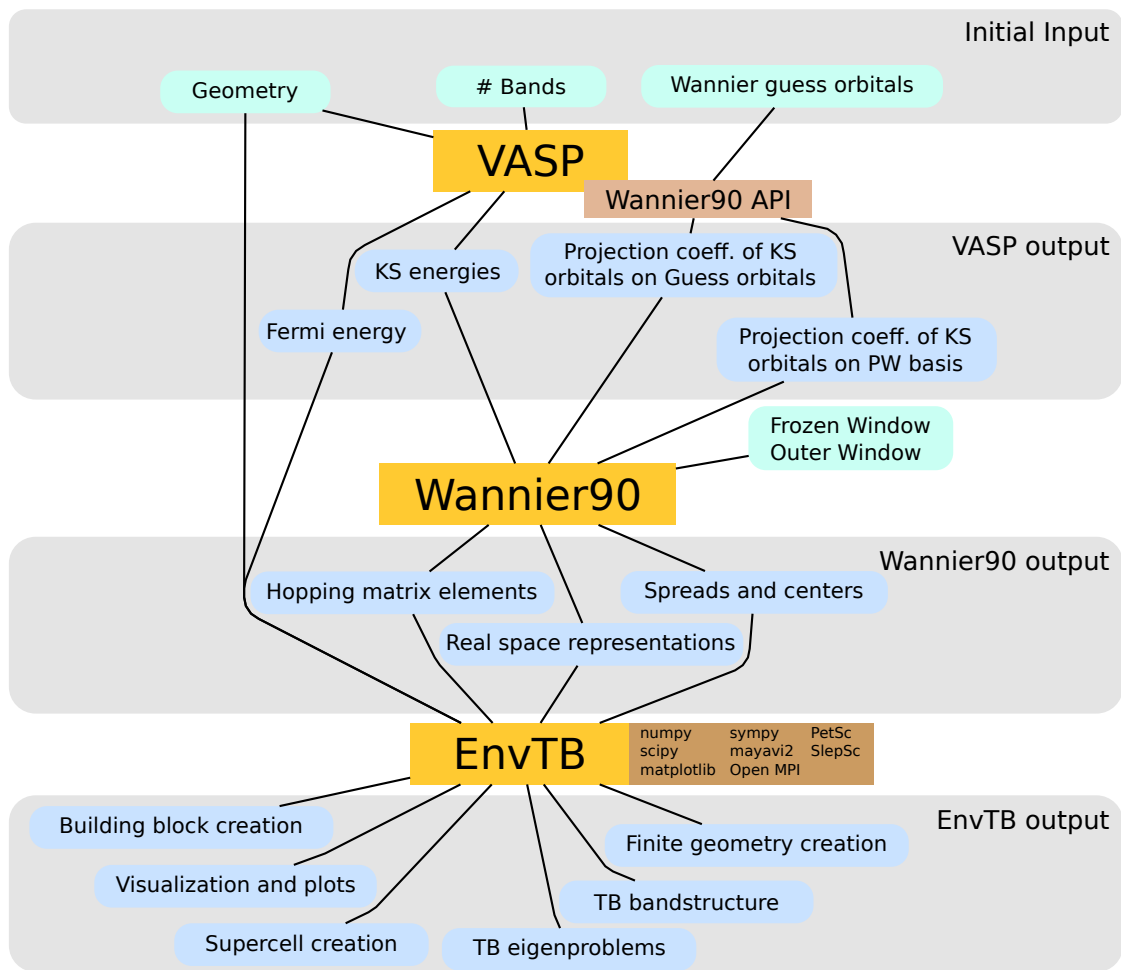


Figure A.1.: Software flowchart

Bibliography

- [1] F. Aquilante. Ridding of factorial scaling in quantum chemistry: the road not taken. *Electronic Structure Theory for Strongly Correlated Systems (Conference)*, Palermo, Italy, 2012.
- [2] N.W. Ashcroft and D.N. Mermin. *Festkörperphysik*. Oldenbourg, 2007.
- [3] Salvador Barraza-Lopez, Markus Kindermann, and M. Y. Chou. Charge transport through graphene junctions with wetting metal leads. *Nano Lett.*, 12(7):3424–3430, June 2012.
- [4] Bruno Dlubak, Marie-Blandine Martin, Robert S. Weatherup, Heejun Yang, Cyrile Deranlot, Raoul Blume, Robert Schloegl, Albert Fert, Abdelmadjid Anane, Stephan Hofmann, Pierre Seneor, and John Robertson. Graphene-Passivated nickel as an Oxidation-Resistant electrode for spintronics. *ACS Nano*, 6(12):10930–10934, November 2012.
- [5] Tian Fang, Aniruddha Konar, Huili Xing, and Debdeep Jena. Carrier statistics and quantum capacitance of graphene sheets and ribbons. *Applied Physics Letters*, 91(9):092109+, 2007.
- [6] M. Finnis. *Interatomic Forces in Condensed Matter*. Oxford Series on Materials Modelling. Oxford University Press, Incorporated, 2010.
- [7] J. Güttinger, F. Molitor, C. Stampfer, S. Schnez, A. Jacobsen, S. Dröscher, T. Ihn, and K. Ensslin. Transport through graphene quantum dots. *Reports on Progress in Physics*, 75(12):126502+, December 2012.
- [8] J. Güttinger, C. Stampfer, F. Libisch, T. Frey, J. Burgdörfer, T. Ihn, and K. Ensslin. Electron-Hole crossover in graphene quantum dots. *Physical Review Letters*, 103(4):046810+, July 2009.
- [9] F. Jensen. *Introduction to computational chemistry*. John Wiley & Sons, 2007.
- [10] V. M. Karpan, G. Giovannetti, P. A. Khomyakov, M. Talanana, A. A. Starikov, M. Zwierzycki, J. van den Brink, G. Brocks, and P. J. Kelly. Graphite and graphene as perfect spin filters. *Physical review letters*, 99(17), October 2007.
- [11] C. Kittel. *Einführung in die Festkörperphysik*. Oldenbourg Verl., 2006.

- [12] Young S. Lee, Marco B. Nardelli, and Nicola Marzari. Band structure and quantum conductance of nanostructures from maximally localized wannier functions: The case of functionalized carbon nanotubes. *Physical Review Letters*, 95:076804+, August 2005.
- [13] F. Libisch. *Electronic structure and transport in mesoscopic devices (PhD thesis)*.
- [14] F. Libisch, S. Rotter, and J. Burgdörfer. Coherent transport through graphene nanoribbons in the presence of edge disorder. *New Journal of Physics*, 14(12):123006+, December 2012.
- [15] F. Libisch, S. Rotter, J. Güttinger, C. Stampfer, and J. Burgdörfer. Transition to landau levels in graphene quantum dots. *Physical Review B*, 81:245411+, June 2010.
- [16] Florian Libisch, Christoph Stampfer, and Joachim Burgdörfer. Graphene quantum dots: Beyond a dirac billiard. *Physical Review B*, 79(11):115423+, March 2009.
- [17] Jesse Maassen, Wei Ji, and Hong Guo. Graphene spintronics: The role of ferromagnetic electrodes. *Nano Lett.*, 11(1):151–155, December 2010.
- [18] Donald W. Marquardt. An algorithm for Least-Squares estimation of nonlinear parameters. *Journal of the Society for Industrial and Applied Mathematics*, 11(2):431–441, June 1963.
- [19] Nicola Marzari, Arash A. Mostofi, Jonathan R. Yates, Ivo Souza, and David Vanderbilt. Maximally localized wannier functions: Theory and applications. *Computational Materials Science*, 61:266–269, May 2012.
- [20] Nicola Marzari and David Vanderbilt. Maximally localized generalized wannier functions for composite energy bands. *Physical Review B*, 56(20):12847–12865, November 1997.
- [21] F. Mittendorfer, A. Garhofer, J. Redinger, J. Klimeš, J. Harl, and G. Kresse. Graphene on ni(111): Strong interaction and weak adsorption. *Physical Review B*, 84(20):201401+, November 2011.
- [22] F. Molitor, J. Güttinger, C. Stampfer, S. Dröscher, A. Jacobsen, T. Ihn, and K. Ensslin. Electronic properties of graphene nanostructures. *Journal of Physics: Condensed Matter*, 23(24):243201+, June 2011.
- [23] A. H. Castro Neto, F. Guinea, N. M. R. Peres, K. S. Novoselov, and A. K. Geim. The electronic properties of graphene. *Reviews of Modern Physics*, 81(1):109–162, January 2009.
- [24] K. S. Novoselov, A. K. Geim, S. V. Morozov, D. Jiang, M. I. Katsnelson, I. V. Grigorieva, S. V. Dubonos, and A. A. Firsov. Two-dimensional gas of massless dirac fermions in graphene. *Nature*, 438(7065):197–200, November 2005.

- [25] K. S. Novoselov, A. K. Geim, S. V. Morozov, D. Jiang, Y. Zhang, S. V. Dubonos, I. V. Grigorieva, and A. A. Firsov. Electric field effect in atomically thin carbon films. *Science*, 306(5696):666–669, October 2004.
- [26] K. S. Novoselov, E. McCann, S. V. Morozov, V. I. Fal’ko, M. I. Katsnelson, U. Zeitler, D. Jiang, F. Schedin, and A. K. Geim. Unconventional quantum hall effect and berry/’s phase of $2[\pi]$ in bilayer graphene. *Nat Phys*, 2(3):177–180, March 2006.
- [27] R.G. Parr and W. Yang. *Density-functional theory of atoms and molecules*. International series of monographs on chemistry. Oxford University Press, 1994.
- [28] Felix Plasser, Hasan Pašalić, Martin H. Gerzabek, Florian Libisch, Rafael Reiter, Joachim Burgdörfer, Thomas Müller, Ron Shepard, and Hans Lischka. Der multi-radikalcharakter ein- und zweidimensionaler Graphen-Nanobänder. *Angew. Chem.*, 125(9):2641–2644, February 2013.
- [29] S. Reich, J. Maultzsch, C. Thomsen, and P. Ordejón. Tight-binding description of graphene. *Physical Review B*, 66(3):035412+, July 2002.
- [30] R. Reiter. *Environment-dependent tight-binding description of polycyclic aromatic hydrocarbons and graphene (project report)*.
- [31] R. Reiter, U. Derra, S. Birner, B. Terrés, F. Libisch, J. Burgdörfer, and C. Stampfer. Negative quantum capacitance in graphene nanoribbons with lateral gates, January 2014.
- [32] S. Das Sarma, Shaffique Adam, E. H. Hwang, and Enrico Rossi. Electronic transport in two-dimensional graphene. *Reviews of Modern Physics*, 83(2):407–470, May 2011.
- [33] Matthew Shelley, Nicolas Poilvert, Arash A. Mostofi, and Nicola Marzari. Automated quantum conductance calculations using maximally-localised wannier functions. January 2011.
- [34] J. C. Slater and G. F. Koster. Simplified LCAO method for the periodic potential problem. *Physical Review Online Archive (Prola)*, 94(6):1498–1524, June 1954.
- [35] Young W. Son, Marvin L. Cohen, and Steven G. Louie. Energy gaps in graphene nanoribbons. *Physical Review Letters*, 97(21):216803+, November 2006.
- [36] Ivo Souza, Nicola Marzari, and David Vanderbilt. Maximally localized wannier functions for entangled energy bands. *Physical Review B*, 65(3):035109+, December 2001.
- [37] C. Stampfer, E. Schurtenberger, F. Molitor, J. Güttinger, T. Ihn, and K. Ensslin. Tunable graphene single electron transistor. *Nano Lett.*, 8(8):2378–2383, July 2008.

- [38] D. Subramaniam, F. Libisch, Y. Li, C. Pauly, V. Geringer, R. Reiter, T. Mashoff, M. Liebmann, J. Burgdörfer, C. Busse, T. Michely, R. Mazzarello, M. Pratzer, and M. Morgenstern. Wave-Function mapping of graphene quantum dots with soft confinement. *Physical Review Letters*, 108:046801+, January 2012.
- [39] A.P. Sutton. *Electronic structure of materials*. Oxford science publications. Clarendon Press, 1993.
- [40] A. Szabó and N.S. Ostlund. *Modern Quantum Chemistry: Introduction to Advanced Electronic Structure Theory*. Dover Books on Chemistry Series. Dover Publications, 1996.
- [41] Wikipedia. Cubic crystal system — Wikipedia, the free encyclopedia, 2006.
- [42] Wikipedia. Density of states — Wikipedia, the free encyclopedia, 2008.